The growth of the central Andes, 22°S–26°S

J. Quade*
M.P. Dettinger
B. Carrapa
P. DeCelles
K.E. Murray
Department of Geosciences, University of Arizona, Tucson, Arizona 85721, USA

K.W. Huntington
Department of Earth and Space Sciences, University of Washington, Seattle, Washington 98195-1310, USA

A. Cartwright
Mintec, Inc., 3544 East Fort Lowell Road, Tucson, Arizona 85716, USA

R.R. Canavan
Department of Geology, University of Wyoming, Laramie, Wyoming 82071, USA

G. Gehrels
Department of Geosciences, University of Arizona, Tucson, Arizona 85721, USA

M. Clementz
Department of Geology, University of Wyoming, Laramie, Wyoming 82071, USA

ABSTRACT

We synthesize geologic observations with new isotopic evidence for the timing and magnitude of uplift for the central Andes between 22°S and 26°S since the Paleocene. To estimate paleoelevations, we used the stable isotopic composition of carbonates and volcanic glass, combined with another paleoelevation indicator for the central Andes: the distribution of evaporites. Paleoelevation reconstruction using clumped isotope paleothermometry failed due to resetting during burial.

The Andes at this latitude rose and broadened eastward in three stages during the Cenozoic. The first, in what is broadly termed the "Incaic" orogeny, ended by the late Eocene, when magmatism and deformation had elevated to ≥4 km the bulk (~50%) of what is now the western and central Andes. The second stage witnessed the gradual building of the easternmost Puna and Eastern Cordillera, starting with deformation as early as 38 Ma, to >3 km by no later than 15 Ma. The proximal portions

*quadej@email.arizona.edu

of the Paleogene foreland basin system were incorporated into the orogenic edifice, and basins internal to the orogen were enclosed and isolated from easterly moisture sources, promoting the precipitation of evaporites. In the third orogenic stage during the Pliocene–Pleistocene, Andean deformation accelerated and stepped eastward to form the modern Subandes, accounting for the final ~15%–20% of the current cross section of the Andes. About 0.5 km of elevation was added unevenly to the Western Cordillera and Puna from 10 to 2 Ma by voluminous volcanism.

The two largest episodes of uplift and eastward propagation of the orogenic front and of the foreland flexural wave, ca. 50 (?)–40 Ma and <5 Ma, overlap with or immediately postdate periods of very rapid plate convergence, high flux magmatism in the magmatic arc, and crustal thickening. Uplift does not correlate with a hypothesized mantle lithospheric foundering event in the early Oligocene. Development of hyperaridity in the Atacama Desert by the mid-Miocene postdates the two-step elevation gain to >3 km of most (~75%) of the Andes. Hence, the record suggests that hyperarid climate was a consequence, not major cause, of uplift through trench sediment starvation.

INTRODUCTION

The Puna-Altiplano is the highest-elevation region of the world not built by continent-continent collision. The development of this high region has preoccupied geologists for generations (e.g., Steinmann, 1929; Mégard, 1984), and as a result, much is known about the timing and extent of the deformation and depositional history. New developments in geochronology, thermochronology, and most recently paleoaltimetry are revolutionizing our view of Andean orogeny, but also stirring debate.

There are several different views of the chronology, spatial patterns, and causes of Andean uplift, based mostly on study of the geology of the Altiplano and adjacent areas. One view holds that deformation and volcanism had raised the western Andes and Altiplano by the Oligocene to mid-Miocene (Horton, 1999; Hoke and Garzione, 2008; Evenstar et al., 2009; Jordan et al., 2010), and subsequently deformation broadened eastward (Horton, 1999; Barnes et al., 2012). Others suggest that the whole of the Andes rose as a single mass, either gradually starting in the Miocene (Ehlers and Poulsen, 2009), or more abruptly in the late Miocene (Kay and Gordillo, 1994; Ghosh et al., 2006a; Garzione et al., 2006, 2008; Gregory-Wodzicki, 2000). One cause of abrupt uplift is thought to be removal of the mantle lithosphere beneath the Andes, either gradually by ablative removal (Pope and Willet, 1998), or abruptly by foundering of eclogitized mantle lithosphere (Garzione et al., 2006, 2008). Others explain late Miocene uplift by ductile lower-crustal flow and underthrusting (Allmendinger and Gubbels, 1996; Barke and Lamb, 2006). Sobel et al. (2003) and Strecker et al. (2007) stressed the role of Neogene orographic barrier development and climatic controls on sediment removal from the orogenic belt in expanding Andean topography. Yet another hypothesis suggests that global cooling in the mid- to late Miocene and attendant aridification of the Atacama Desert raised the Andes, due to the high shear stresses that developed as a result of trench starvation of sedi-

ment (Lamb and Davis, 2003). Studies have provided extensive geologic and thermochronologic evidence for deformation and exhumation, but only a few attempt to quantify paleoelevations achieved by this deformation. Evenstar et al. (2009) and Jordan et al. (2010) interpreted tilting of surfaces and ignimbrite flows to indicate that the western slope of the Andes stood ~2000 m above the adjacent forearc (now at ~1–1.5 km) by the early to mid-Miocene, and it has added a further ~1 km since then. Using isotopic evidence, Ghosh et al. (2006a) and Garzione et al. (2006, 2008) suggested that the whole of the Andes at the latitude of the Altiplano rose from ≤2 km to ~4 km between 10 and 5 Ma. Ehlers and Poulsen (2009) reinterpreted some of this same evidence to suggest the Andes also rose en masse, but more slowly, starting in the early Miocene. Recently, papers by many of the same authors show more convergence of views, with the recognition that uplift was probably time transgressive, west to east (e.g., Hoke and Garzione, 2008; Barnes et al., 2012).

Haschke et al. (2006) viewed the development of the Andes as a cyclical process involving gradual crustal thickening, deep lithospheric foundering, and slab shallowing, culminating in regional uplift. DeCelles et al. (2009) presented a holistic model in which crustal shortening, magmatism, upper-mantle dripping/delamination of dense eclogitic instabilities created by shortening and magmatism, and surface uplift are all linked. These processes operate on a cyclical schedule to build cordilleran-style orogenic belts such as the North and South American Cordilleras. The South American cycles are hypothesized to last 25–30 m.y. and are predicted to have culminated in Andean uplift during the early Oligocene and possibly the latest Neogene (Haschke et al., 2006).

In this paper, we journey south of the Altiplano to the Puna Plateau and the 22°S–26°S sector of the Andes (Fig. 1). For this sector, we merge the geologic and thermochronologic evidence for deformation with the gradual development of high elevations of the region. For paleoaltimetry, we rely on a large suite of new

isotopic evidence from carbonates and volcanic glass, as well as from the new clumped isotope geothermometer. We use the modern distribution of salt lakes in South America for additional constraints on paleoelevation. Most reconstructions of surface elevation change have tended to focus on tectonic rather than volcanic contributions. Volcanic rocks have a conspicuous presence in the Andes, and to complete the picture of surface elevation changes, their contribution must be considered, especially during the last 10 m.y. In the final part of this paper, we turn to likely causes of Andean deformation and uplift during the Cenozoic.

GEOGRAPHIC AND GEOLOGICAL BACKGROUND

Physiographic and Climate Divisions

The modern Andes can be conveniently divided into five physio-tectonic zones from east to west between 22°S and 26°S: the Subandes, the Eastern Cordillera, and the Puna Plateau in the retroarc; the magmatic arc in the Western Cordillera; and the Atacama Desert in the forearc (Fig. 1). The Subandes (or more locally the Santa Bárbara system) at this latitude consist of a series of variably elevated (<5 km) frontal ranges dividing externally drained, relatively low-elevation (<1 km) basins. The Subandes below 2 km are heavily vegetated, being fed by rains >1 m/yr carried by the prevailing easterlies (Zhou and Lau, 1998; Strecker et al., 2007). Above 2 km elevation, rainfall decreases rapidly. The Subandes ascend into the Eastern Cordillera, which attains elevations of >6 km. The Eastern Cordillera bounds the eastern edge of the Puna Plateau, hydrographically isolating the Puna basins and blocking the easterlies at this latitude. The Eastern Cordillera and Subandes are underlain by mainly Proterozoic and Lower Paleozoic clastic sedimentary rocks and Ordovician granitoids. These are locally capped by Cretaceous-age rift deposits of the Salta Group, and above them, by thick Cenozoic foreland basin deposits.

The Puna Plateau is the southern extension of the central Andean Plateau; the Altiplano Plateau in Bolivia forms the broader northern extension. The Puna Plateau stands at ~4 km average elevation, and the climate is arid to hyperarid due to partial interdiction of easterly moisture by the Eastern Cordillera. The Puna Plateau consists of N-S–trending basins bounded by thrust faults and filled by coarse clastic rocks and evaporites.
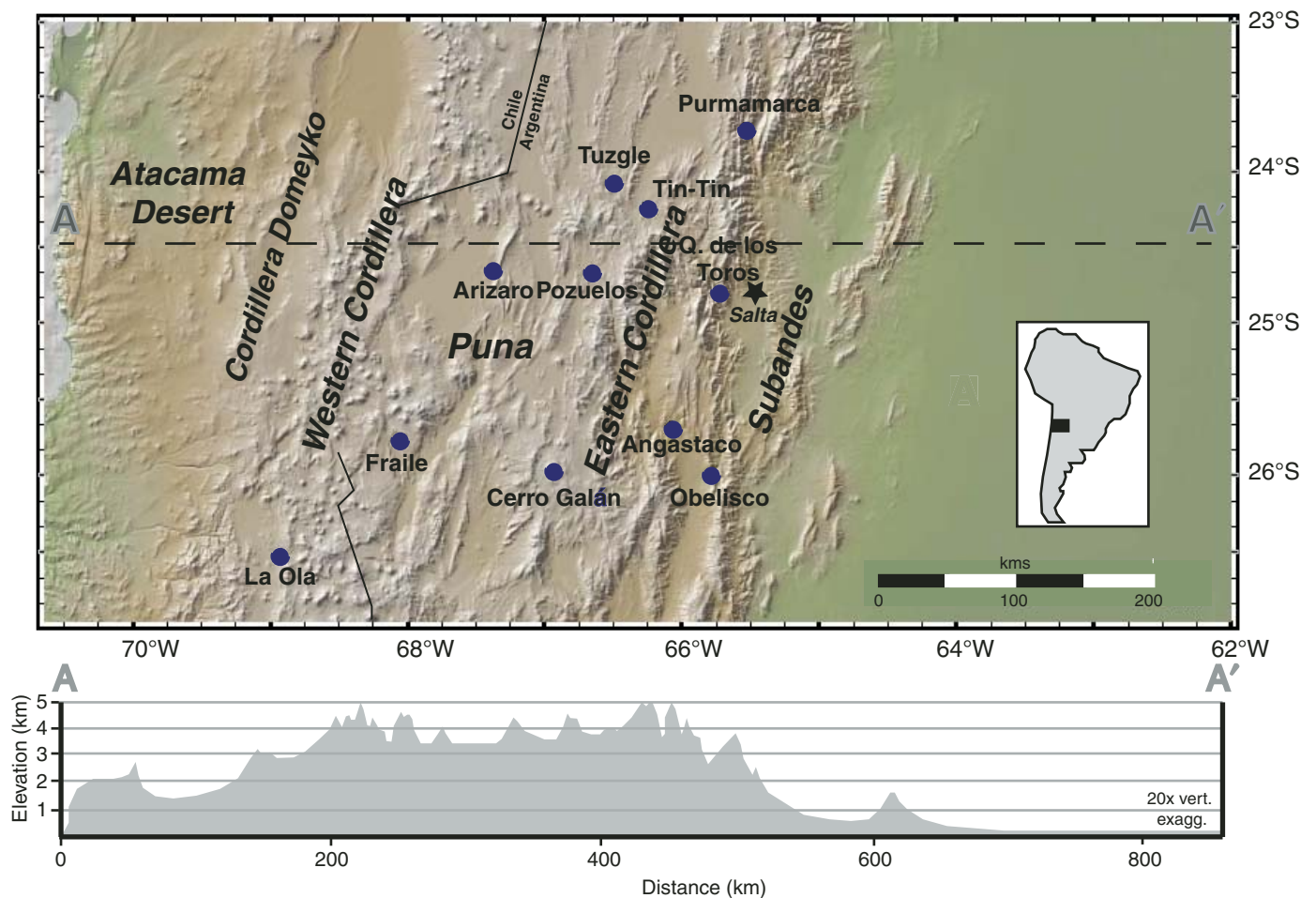

Figure 1. The major physiographic provinces of the central Andes and the main study locations.

The ranges reach >6 km elevations and are dominated by Lower Paleozoic sedimentary and igneous rocks; Cenozoic sedimentary rocks and volcanic rocks, including many voluminous late Neogene–age ignimbrites, are also widespread.

Bounding the western Puna region, the Western Cordillera is the main magmatic arc of the Andes. The arc consists of stratovolcanoes, flows, and ignimbrite sheets perched on top of the western edge of the otherwise moderate-relief Puna. Arid to hyperarid conditions prevail due to the nearly complete interdiction of the easterlies by the eastern Andes.

The Atacama Desert, a Martian-like region that is driest in this sector at 24°S–26°S, lies in the forearc west of the Andes. The forearc is underlain by Eocene and older intrusive, extrusive, and metasedimentary rocks, capped by mainly Neogene coarse clastic sedimentary rocks, evaporites, ignimbrites, and tephras.

Geologic Background and Sampling 22°S–26°S

The geologic history of this sector of the Andes has been substantially revised and expanded in the past few decades. The duration and locations of deformation and magmatism are sufficiently understood that we can compare this record to our evidence for the development of paleoelevation across the region. Here, we describe our sampling campaign in the context of a brief summary of the geologic evolution of the Andes at 22°S–26°S since the Late Cretaceous, where the geologic record is most complete.

The western margin of the central Andes between 22°S and 26°S has undergone some form of subduction and compression since the opening of the South Atlantic during the Early Cretaceous (Torsvik et al., 2009). In response, deformation (and uplift?) of the Andes at this and adjacent latitudes began in the west and gradually expanded eastward. This eastward progression is visible in a variety of structural (Mpodozis et al., 2005; Hongn et al., 2007; DeCelles et al., 2011; Carrapa et al., 2011b), paleotopographic and provenance (Hain et al., 2011; DeCelles et al., 2011), and thermochronologic (Deeken et al., 2006; Coutand et al., 2006; Carrapa and DeCelles, 2008; Carrapa et al., 2011b; Carrapa and DeCelles, this volume; Reiners et al., this volume) evidence. During the Eocene, a combination of arc magmatism and deformation created what we will term the "Incaic highlands," which stretched from the Cordillera de Domeyko in Chile eastward probably across much of the Puna Plateau (Fig. 1; Mpodozis et al., 2005; Trumbull et al., 2006; DeCelles et al., 2007; Carrapa et al., 2011b). To reconstruct absolute paleoelevations of the Incaic highlands, we used the δD value of waters of hydration in volcanic glass. This approach has been employed successfully in the western North American Cordillera to reconstruct Cenozoic paleoelevations (Mulch et al., 2008; Cassel et al., 2009). The method requires δD analysis of waters sealed in hydration rinds of volcanic glass to reconstruct the δD value of ancient water, which in turn is a function of elevation. We analyzed well-preserved glass from numerous ash-fall tuffs in basin deposits around Salar de Fraile and Salar de Arizaro in western

Argentina (Fig. 1). U-Pb dating of volcanic zircons in these tuffs provided the age control on our paleoelevation reconstructions from these tuffs.

During the Paleogene, a broad foreland basin stretched eastward of the Western Cordillera and Cordillera de Domeyko (the "Incaic highlands"), starting at about of 67°W. Thick deposits belonging the Santa Bárbara and Metán Subgroups were shed from the highlands eastward into the foreland basin (Fig. 2; DeCelles et al., 2011; Carrapa et al., 2011a). These deposits contain abundant surficial carbonate, the isotopic composition of
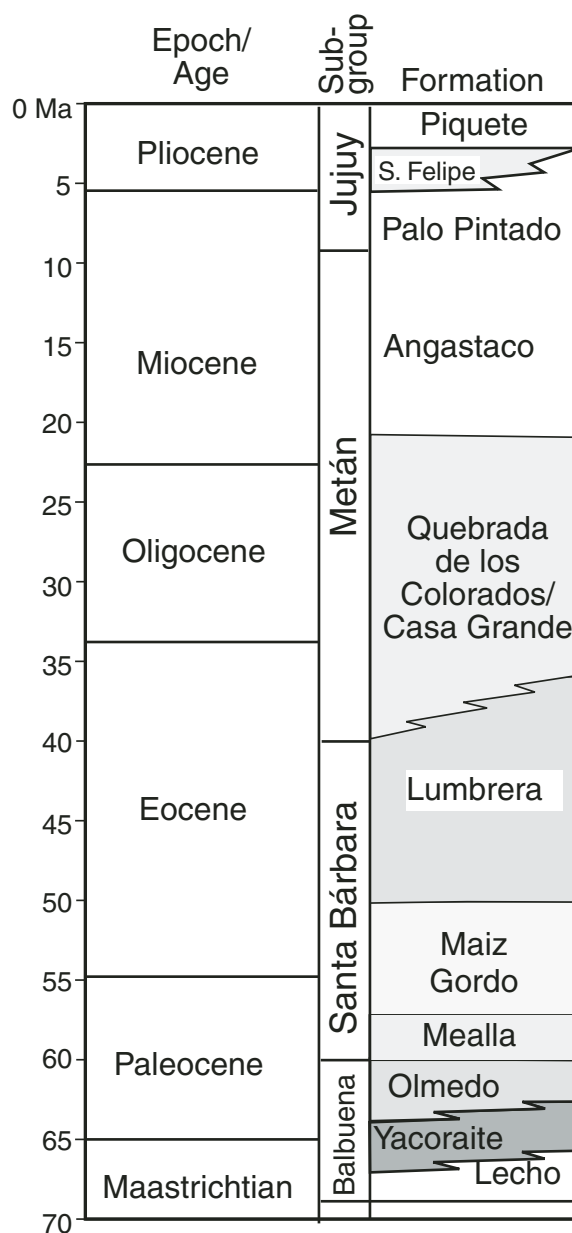

Figure 2. Stratigraphic chart of the eastern Puna and Cordillera, and Subandean zone of northwestern Argentina, modified from DeCelles et al. (2011).

which, if not reset during diagenesis, should record low-elevation paleoenvironments of the time. For this paper, we sampled paleosol carbonate nodules (Fig. 3B) from the back-bulge deposits of the Mealla and Maiz Gordo Formations (Santa Barbara Group) at the Obelisco (Fig. 3A), Tin-Tin, and San Antonio de los Cobres sections (Fig. 3C); and the foredeep deposits of the Quebrada de los Colorados Formation (Métan Subgroup) at the San Antonio de los Cobres and Tin-Tin sections (Fig. 1). Paleosol carbonate is abundant in these formations, providing a means of establishing the low-elevation isotopic composition of paleorainfall ($\delta^{18}O$), paleotemperature (Δ_{47}), and paleovegetation ($\delta^{13}C$). Together, these records allow us to correct our paleoelevation reconstructions of the Incaic highlands for any major changes in paleoclimate during the Paleogene.

Deformation and uplift spread eastward during the Neogene, raising the proximal portion of the former foreland up into what is now the Eastern Cordillera and Subandes. Again, volcanic glass is widely available to chronicle these changes and establish absolute paleoelevations, sampled from in and around Tuzgle, Cerro Galàn, La Ola, San Antonio de los Cobres, and other locations (Fig. 1). Geologic evidence for hydrographic isolation and aridification of montane basins, also compiled here, assists in reconstructing the eastward expansion and uplift of the eastern Andes during the Neogene.

METHODS

Isotopic Analysis of Carbonate

Pedogenic carbonates were scraped from alluvial or bedrock clasts or sampled from nodules. Carbonate analyzed for $\delta^{18}O$ and $\delta^{13}C$ values was heated at 250 °C for 3 h in vacuo before stable isotopic analysis using an automated sample preparation device (Kiel III) attached directly to a Finnigan MAT 252 mass spectrometer at the University of Arizona. Measured $\delta^{18}O$ and $\delta^{13}C$ values were corrected using internal laboratory standards calibrated to NBS-19. Precision of repeated standards is ±0.11‰ for $\delta^{18}O$ (1σ). Carbonate isotopic results are reported using standard delta per mil notation relative to Vienna Peedee belemnite (VPDB; Table 1).

Carbonate was analyzed for clumped isotope (Δ_{47}) thermometry at the California Institute of Technology. Samples were digested in phosphoric acid at 90 °C and purified using an automated sample preparation device coupled to a Thermo MAT 253 mass spectrometer configured to measure m/z 44–49 (Eiler and Schauble, 2004), following the methods of Passey et al. (2010). Measured Δ_{47} values were normalized and corrected for scale compression using heated gases (Huntington et al., 2009), corrected for 90 °C acid digestion (0.081‰; Passey et al., 2010), and converted to the absolute reference frame (Dennis et al., 2011) using heated CO_2 and carbonate standards (see GSA Data Repository for details[1]). Corrected Δ_{47} values were converted to temperature using both the Caltech (Ghosh at al., 2006b) and Harvard (Dennis and Schrag, 2010) calibration curves, translated to the absolute reference frame by Dennis et al. (2011). Temperature estimates ($T\Delta_{47}$) and $\delta^{18}O$ and $\delta^{13}C$ values of carbonate (VPDB) from clumped isotope measurements are summarized in Table 2, along with estimates of the $\delta^{18}O$ values (relative to Vienna standard mean ocean water [VSMOW]) of water calculated from the measured carbonate ($T\Delta_{47}$) and $\delta^{18}O$ values using the equation of Kim and O'Neil (1997). Temperatures discussed in the text were calculated using the Caltech calibration, with temperatures calculated using the Harvard calibration in parentheses.

Isotopic Analysis of Volcanic Glass

Each 100–200 g sample of tuff (air-fall or ash-flow) was purified for analysis following procedures described in Dettinger and Quade (this volume). For analysis, 2–3 mg of glass were packed in silver foil. The δD_{vg} values were determined using an automated thermal conversion/element analyzer (TCEA) coupled to a Delta V Plus isotope ratio mass spectrometer with an analytical precision of ±2.5‰ (2σ). The isotope ratios were calibrated using an internal standard and the international standards NBS-30 biotite and IAEA-CH-7 polyethylene foil. All δD values are reported here in standard delta notation and referenced to SMOW (Table 3).

Age Control

The ages of ash-fall and ash-flow tuffs were determined by U-Pb dating of volcanic zircons. Grain ages were determined by multicollector–laser ablation–inductively coupled plasma–mass spectrometry (MC-LA-ICP-MS) at the University of Arizona LaserChron Center. Individual zircon grains were ablated with a New Wave DUV193 Excimer laser (operating at a wavelength of 193 nm) using a spot diameter of 35 µm. The ablated material is carried in He gas into the plasma source of a Micromass Isoprobe, which is equipped with a flight tube of sufficient width that U, Th, and Pb isotopes are measured simultaneously. All measurements were made in static mode, using Faraday detectors for ^{238}U, ^{232}Th, ^{208}Pb–^{206}Pb, and an ion-counting channel for ^{204}Pb. Ion yields were ~1 mv per ppm. Each analysis consisted of one 20 s integration on peaks with the laser off (for backgrounds), twenty 1 s integrations with the laser firing, and a 30 s delay to purge the previous sample and prepare for the next analysis. The ablation pit was ~20 m deep. Common Pb correction was made by using the measured ^{204}Pb and assuming an initial Pb composition from Stacey and Kramers (1975) (with uncertainties of 1.0 for $^{206}Pb/^{204}Pb$ and 0.3 for $^{207}Pb/^{204}Pb$). Our measurement of ^{204}Pb was unaffected by the presence of ^{204}Hg because backgrounds were measured on peaks (thereby subtracting any background

---

[1]GSA Data Repository Item 2015007, Heated gas and carbonate standard data used to standardize clumped isotope data (Huntington et al., 2009) and convert data to the absolute reference frame (Dennis et al., 2011), is available at www.geosociety.org/pubs/ft2015.htm, or on request from editing@geosociety.org or Documents Secretary, GSA, P.O. Box 9140, Boulder, CO 80301-9140, USA.
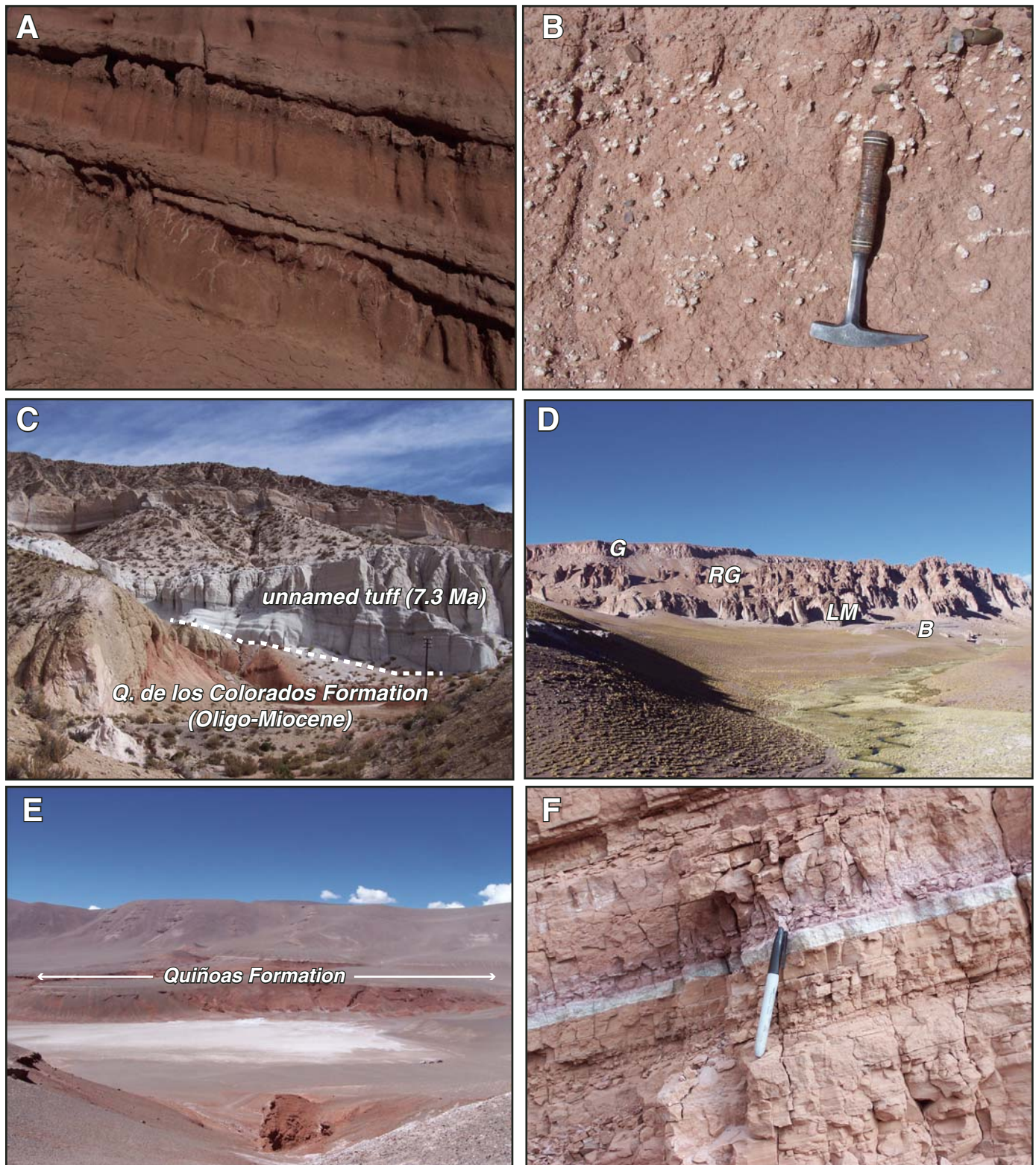
Figure 3. Examples of materials and locations sampled for paleoelevation reconstruction. (A) Stacked vertisols from the Mealla-Maiz Gordo Formation at Obelisco (Fig. 1). These paleosols contain abundant soil carbonate. (B) Detail of soil carbonate nodules from the red beds in part C. (C) Exposure near San Antonio de los Cobres (Fig. 1) showing red beds of the Quebrada de los Colorados Formation at the bottom of the photo, and above that, Neogene tuffs resting on the red beds along an angular unconformity. The basal white tuff dates to 7.3 Ma (see Table 3, SL-41). (D) Stacked ignimbrites of Neogene age near Cerro Galán sampled for δD analysis of volcanic glass: Blanco (B), the lower Merihuaca (LM), the Real Grande (RG), and the Galán (G) ignimbrites (see Table 3). (E) View of the Salar de Fraile Basin (Fig. 1). The red beds in the background belong to the Quiñoas Formation and contain evaporites as far back as the late Eocene. (F) Detail of ash-fall tuff with well-preserved glass in the Eocene–Oligocene Quiñoas Formation at Salar de Fraile.

TABLE 1. STABLE ISOTOPIC RESULTS FROM CARBONATES

Samples	Formation	Location	Latitude (°S)	Longitude (°W)	Elevation (m)	Local thickness (m)	$\delta^{13}C$ (‰, PDB)	$\delta^{18}O$ (‰, PDB)	Age (Ma)	Material
SL44A	Mealla Fm.	Obelisco	25.98330	65.74860	1540	3	−6.24	−4.29	61	Stromatolite
SL44B	Mealla Fm.	Obelisco	25.98330	65.74860	1540	3	−3.55	−3.83	61	Stromatolite
SL44c	Mealla Fm.	Obelisco	25.98330	65.74860	1540	3	−2.14	−7.95	61	Stromatolite
SL44D	Mealla Fm.	Obelisco	25.98330	65.74860	1552	14	−3.43	−6.79	61	Intraclastic breccias
SL-45C(A)	Mealla Fm. ?	Obelisco	26.00064	65.78368	1558	272	−9.05	−5.63	63	Vertisol carbonate
SL-45C(B)	Mealla Fm. ?	Obelisco	26.00064	65.78368	1558	272	−9.10	−5.93	63	Vertisol carbonate
SL-45F(A)	Mealla Fm. ?	Obelisco	26.00064	65.78368	1558	280	−9.82	−6.27	63	Vertisol carbonate
SL-45F(B)	Mealla Fm. ?	Obelisco	26.00064	65.78368	1558	280	−9.11	−5.91	63	Vertisol carbonate
SL-45A(A)	Mealla Fm. ?	Obelisco	26.00064	65.78368	1558	267	−9.23	−5.67	63	Vertisol carbonate
SL-45A(B)	Mealla Fm. ?	Obelisco	26.00064	65.78368	1558	267	−9.04	−6.07	63	Vertisol carbonate
SL-45A(C)	Mealla Fm. ?	Obelisco	26.00064	65.78368	1558	267	−8.43	−6.03	63	Vertisol carbonate
SL-45D(A)	Mealla Fm. ?	Obelisco	26.00064	65.78368	1558	275	−9.36	−6.01	63	Vertisol carbonate
SL-45D(B)	Mealla Fm. ?	Obelisco	26.00064	65.78368	1558	275	−8.81	−5.63	63	Vertisol carbonate
SL-45B(A)	Mealla Fm. ?	Obelisco	26.00064	65.78368	1558	271	−8.72	−5.56	63	Vertisol carbonate
SL-45B(B)	Mealla Fm. ?	Obelisco	26.00064	65.78368	1558	271	−8.69	−5.38	63	Vertisol carbonate
SL-45E(A)	Mealla Fm. ?	Obelisco	26.00064	65.78368	1558	278	−8.58	−5.92	63	Vertisol carbonate
SL-45E(B)	Mealla Fm. ?	Obelisco	26.00064	65.78368	1558	278	−8.46	−5.85	63	Vertisol carbonate
SL-47A	Mealla Fm. ?	Obelisco	26.01087	65.78390	1563	110	−7.99	−5.59	63	Vertisol carbonate
SL-47B	Mealla Fm. ?	Obelisco	26.01087	65.78390	1563	110	−8.11	−5.81	63	Vertisol carbonate
SL-47C	Mealla Fm. ?	Obelisco	26.01087	65.78390	1563	110	−7.87	−7.46	63	Vertisol carbonate
SL-59A	Maiz Gordo Fm.	San Antonio	24.22901	66.25286	3850	87	−15.43	−2.99	55	Groundwater calcrete
SL-59B	Maiz Gordo Fm.	San Antonio	24.22901	66.25286	3850	87	−15.65	−2.56	55	Groundwater calcrete
SL-60B	Maiz Gordo Fm.	San Antonio	24.22906	66.25277	3840	97.5	−15.17	−4.37	55	Groundwater calcrete
SL-60C	Maiz Gordo Fm.	San Antonio	24.22906	66.25277	3840	97.5	−9.06	−2.48	55	Groundwater calcrete
SL-61A	Maiz Gordo Fm.	San Antonio	24.22906	66.25277	3840	97.5	−16.05	−2.34	55	Groundwater calcrete
SL-61B	Maiz Gordo Fm.	San Antonio	24.22906	66.25277	3840	97.5	−16.20	−3.36	55	Groundwater calcrete
SL-61C	Maiz Gordo Fm.	San Antonio	24.22906	66.25277	3840	97.5	−16.36	−2.09	55	Groundwater calcrete
SL62	Maiz Gordo Fm.	San Antonio	24.22924	66.25243	3844	124	−13.25	−4.76	55	Groundwater calcrete
SL63	Maiz Gordo Fm.	San Antonio	24.22928	66.25199	3848	154	−10.19	−0.99	55	Reworked soil carbonate

(*Continued*)

TABLE 1. STABLE ISOTOPIC RESULTS FROM CARBONATES (*Continued*)

Samples	Formation	Location	Latitude (°S)	Longitude (°W)	Elevation (m)	Local thickness (m)	$\delta^{13}C$ (‰, PDB)	$\delta^{18}O$ (‰, PDB)	Age (Ma)	Material
SL64	Maiz Gordo Fm.	San Antonio	24.22928	66.25199	3848	154	−3.78	−9.36	55	Reworked soil carbonate
SL65	Maiz Gordo Fm.	San Antonio	24.22936	66.25187	3849	161	−6.57	−2.62	55	Reworked soil carbonate
SL68	Maiz Gordo Fm.	San Antonio	24.22973	66.25157	3853	188	−8.66	−3.18	55	Soil carbonate
SL69	Maiz Gordo Fm.	San Antonio	24.22973	66.25157	3853	190	−9.83	−7.48	55	Soil carbonate
SL-70A	Maiz Gordo Fm.	San Antonio	24.22973	66.25157	3853	194	−7.41	−2.59	55	Soil carbonate
SL-70B	Maiz Gordo Fm.	San Antonio	24.22973	66.25157	3853	194	−7.79	−2.76	55	Soil carbonate
SL-70C	Maiz Gordo Fm.	San Antonio	24.22973	66.25157	3853	194	−7.27	−1.88	55	Soil carbonate
SL-71	Maiz Gordo Fm.	San Antonio	24.23009	66.25122	3864	229	−7.90	−3.50	55	Carbonate in supersol
SL-72	Maiz Gordo Fm.	San Antonio	24.23009	66.25122	3864	221	2.65	−2.72	55	Carbonate in supersol
SL-73A	Maiz Gordo Fm.	San Antonio	24.23009	66.25122	3864	221	−10.47	−8.45	55	Carbonate in supersol
SL-73B	Maiz Gordo Fm.	San Antonio	24.23009	66.25122	3864	221	−10.99	−7.00	55	Carbonate in supersol
SL-73C	Maiz Gordo Fm.	San Antonio	24.23009	66.25122	3864	300	−11.41	−7.46	37	Soil carbonate
SL-74A	Q. de los Colorados	San Antonio, lower	24.23262	66.2457	3847	300	−7.27	−6.92	37	Soil carbonate
SL-74B	Q. de los Colorados	San Antonio, lower	24.23262	66.2457	3847	300	−7.77	−6.73	37	Soil carbonate
SL-74C	Q. de los Colorados	San Antonio, lower	24.23262	66.2457	3847	302	−7.72	−6.74	37	Soil carbonate
SL75	Q. de los Colorados	San Antonio, lower	24.23262	66.2457	3847	400	−7.45	−7.82	37	Soil carbonate
SL-29A	Q. de los Colorados	San Antonio, lower	24.24091	66.24138	3836	400	−8.16	−5.97	37	Soil carbonate
SL-29B	Q. de los Colorados	San Antonio, lower	24.24091	66.24138	3836	400	−8.23	−5.69	37	Soil carbonate
SL-29C	Q. de los Colorados	San Antonio, lower	24.24091	66.24138	3836	410	−8.03	−5.18	37	Soil carbonate
SL-30A	Q. de los Colorados	San Antonio, lower	24.24091	66.24138	3836	410	−7.35	−5.63	37	Soil carbonate
SL-30B	Q. de los Colorados	San Antonio, lower	24.24091	66.24138	3836	410	−7.07	−4.56	37	Soil carbonate
SL-30C	Q. de los Colorados	San Antonio, lower	24.24091	66.24138	3836	410	−7.64	−5.57	37	Soil carbonate
SL-136A-1	Q. de los Colorados	San Antonio, upper	24.23589	66.24085	3837	430	−8.17	−4.11	33	Soil carbonate
SL-136A-2	Q. de los Colorados	San Antonio, upper	24.23589	66.24085	3837	430	−8.53	−4.78	33	Soil carbonate
SL-136A-3	Q. de los Colorados	San Antonio, upper	24.23589	66.24085	3837	430	−8.19	−4.15	33	Soil carbonate
SL-136A-4	Q. de los Colorados	San Antonio, upper	24.23589	66.24085	3837	430	−8.47	−4.58	33	Soil carbonate
SL-136B-1	Q. de los Colorados	San Antonio, upper	24.23589	66.24085	3837	460	−8.08	−4.30	31	Soil carbonate
SL-136B-2	Q. de los Colorados	San Antonio, upper	24.23589	66.24085	3837	460	−8.63	−5.15	31	Soil carbonate
SL-136B-3	Q. de los Colorados	San Antonio, upper	24.23589	66.24085	3837	460	−8.14	−4.57	31	Soil carbonate

(*Continued*)

TABLE 1. STABLE ISOTOPIC RESULTS FROM CARBONATES (*Continued*)

Samples	Formation	Location	Latitude (°S)	Longitude (°W)	Elevation (m)	Local thickness (m)	$\delta^{13}C$ (‰, PDB)	$\delta^{18}O$ (‰, PDB)	Age (Ma)	Material
SL-136B-4	Q. de los Colorados	San Antonio, upper	24.23589	66.24085	3837	460	−8.30	−4.81	31	Soil carbonate
SL-136C-1	Q. de los Colorados	San Antonio, upper	24.23589	66.24085	3837	560	−7.69	−5.47	27	Soil carbonate
SL-136C-2	Q. de los Colorados	San Antonio, upper	24.23589	66.24085	3837	560	−7.91	−4.15	27	Soil carbonate
SL-136C-3	Q. de los Colorados	San Antonio, upper	24.23589	66.24085	3837	560	−7.88	−4.32	27	Soil carbonate
SL-136C-4	Q. de los Colorados	San Antonio, upper	24.23589	66.24085	3837	560	−8.05	−4.36	27	Soil carbonate
SL-135-A1	Q. de los Colorados	Tin-Tin	25.24116	66.07684	2740		−9.02	−6.85	43	Soil carbonate
SL-135-A2	Q. de los Colorados	Tin-Tin	25.24116	66.07684	2740		−9.17	−7.72	43	Soil carbonate
SL-135-A3	Q. de los Colorados	Tin-Tin	25.24116	66.07684	2740		−8.88	−6.51	43	Soil carbonate
SL-135-B1	Q. de los Colorados	Tin-Tin	25.24116	66.07684	2740		−9.18	−6.93	43	Soil carbonate
SL-135-B2	Q. de los Colorados	Tin-Tin	25.24116	66.07684	2740		−9.23	−8.37	43	Soil carbonate
SL-135-B3	Q. de los Colorados	Tin-Tin	25.24116	66.07684	2740		−9.08	−8.02	43	Soil carbonate
SL-135-C1	Q. de los Colorados	Tin-Tin	25.24116	66.07684	2740		−9.52	−6.47	43	Soil carbonate
SL-135-C2	Q. de los Colorados	Tin-Tin	25.24116	66.07684	2740		−9.10	−7.15	43	Soil carbonate
SL-135-C3	Q. de los Colorados	Tin-Tin	25.24116	66.07684	2740		−9.03	−6.75	43	Soil carbonate
SL-135-D1	Q. de los Colorados	Tin-Tin	25.24116	66.07684	2740		−9.11	−6.30	43	Soil carbonate
SL-135-D2	Q. de los Colorados	Tin-Tin	25.24116	66.07684	2740		−9.19	−6.56	43	Soil carbonate
SL-135-D3	Q. de los Colorados	Tin-Tin	25.24116	66.07684	2740		−9.46	−6.63	43	Soil carbonate
SL-135-E1	Q. de los Colorados	Tin-Tin	25.24116	66.07684	2740		−9.39	−5.55	43	Soil carbonate
SL-135-E2	Q. de los Colorados	Tin-Tin	25.24116	66.07684	2740		−8.99	−5.86	43	Soil carbonate
SL-135-E3	Q. de los Colorados	Tin-Tin	25.24116	66.07684	2740		−8.88	−5.89	43	Paleosol nodules
SL-134A-2	Lumbrera supersol	Sierra de Hornocal	23.16314	65.08318	4043		−10.75	−7.55	50	Sandstone cement
SL-134A-3	Lumbrera supersol	Sierra de Hornocal	23.16314	65.08318	4043		−9.11	−14.68	50	Sandstone cement
SL-134A-4	Lumbrera supersol	Sierra de Hornocal	23.16314	65.08318	4043		−8.99	−12.25	50	Sandstone cement
SL-134B-1	Lumbrera supersol	Sierra de Hornocal	23.16314	65.08318	4043		−9.59	−9.56	50	Sandstone cement
SL-134B-2	Lumbrera supersol	Sierra de Hornocal	23.16314	65.08318	4043		−10.61	−8.78	50	Sandstone cement
SL-134B-3	Lumbrera supersol	Sierra de Hornocal	23.16314	65.08318	4043		−9.70	−9.55	50	Sandstone cement
SL-134B-4	Lumbrera supersol	Sierra de Hornocal	23.16314	65.08318	4043		−11.27	−6.54	50	Sandstone cement
SL-134C-1	Lumbrera supersol	Sierra de Hornocal	23.16314	65.08318	4043		−10.17	−9.80	50	Sandstone cement
SL-134C-2	Lumbrera supersol	Sierra de Hornocal	23.16314	65.08318	4043		−10.54	−5.94	50	Sandstone cement

(*Continued*)

TABLE 1. STABLE ISOTOPIC RESULTS FROM CARBONATES (*Continued*)

Samples	Formation	Location	Latitude (°S)	Longitude (°W)	Elevation (m)	Local thickness (m)	$\delta^{13}C$ (‰, PDB)	$\delta^{18}O$ (‰, PDB)	Age (Ma)	Material
SL-134C-3	Lumbrera supersol	Sierra de Hornocal	23.16314	65.08318	4043		−10.66	−5.83	50	Sandstone cement
SL-134C-4	Lumbrera supersol	Sierra de Hornocal	23.16314	65.08318	4043		−10.75	−6.02	50	Sandstone cement
SL-134D-1	Lumbrera supersol	Sierra de Hornocal	23.16314	65.08318	4043		−10.16	−8.31	50	Sandstone cement
SL-134D-2	Lumbrera supersol	Sierra de Hornocal	23.16314	65.08318	4043		−10.27	−9.31	50	Sandstone cement
SL-134D-3	Lumbrera supersol	Sierra de Hornocal	23.16314	65.08318	4043		−11.13	−6.92	50	Sandstone cement
SL-81A	Sijes Fm.	S. Pastos Grandes	24.67004	66.65445	3956		1.49	−1.13	5	Lacustrine siltstone
SL-81B	Sijes Fm.	S. Pastos Grandes	24.67004	66.65445	3956		−1.37	−5.38	5	Lacustrine siltstone
SL-81C	Sijes Fm.	S. Pastos Grandes	24.67004	66.65445	3956		−0.95	−1.52	5	Lacustrine siltstone
SL-89A	Sijes Fm.	S. Pastos Grandes	24.67581	66.65656	3963		9.31	4.76	5	Lacustrine siltstone
SL-89B	Sijes Fm.	S. Pastos Grandes	24.67581	66.65656	3963		7.46	4.44	5	Lacustrine siltstone
SL-90	Sijes Fm.	S. Pastos Grandes	24.67425	66.65434	3955		−3.42	3.70	5	Lacustrine siltstone
SL-91	Pozuelos Fm.	S. Pastos Grandes	24.69445	66.69913	3858		−4.57	−0.33	7	Sandstone cement
SL-92	Pozuelos Fm.	S. Pastos Grandes	24.69415	66.69955	3869		−3.02	1.38	7	Travertine
SL-93	Pozuelos Fm.	S. Pastos Grandes	24.69401	66.69985	3874		−5.12	1.81	7	Travertine
SL-95	Pozuelos Fm.	S. Pastos Grandes	24.69464	66.70111	3865		−3.98	−0.56	7	Travertine
SL-96	Pozuelos Fm.	S. Pastos Grandes	24.69464	66.70111	3865		−3.77	−3.49	7	Travertine
SL-98	Pozuelos Fm.	S. Pastos Grandes	24.69467	66.70199	3857		−3.15	−4.78	7	Travertine
SL-94A	Pozuelos Fm.	S. Pastos Grandes	24.69464	66.70111	3865		−1.98	−3.97	7	Travertine
SL-94B	Pozuelos Fm.	S. Pastos Grandes	24.69464	66.70111	3865		−1.77	−4.22	7	Travertine
SL-94C	Pozuelos Fm.	S. Pastos Grandes	24.69464	66.70111	3865		−1.01	−4.08	7	Travertine
SL-94D	Pozuelos Fm.	S. Pastos Grandes	24.69464	66.70111	3865		−0.93	−4.11	7	Travertine
SL-94E	Pozuelos Fm.	S. Pastos Grandes	24.69464	66.70111	3865		−2.87	−2.07	7	Travertine
SL-94BLACKA	Pozuelos Fm.	S. Pastos Grandes	24.69464	66.70111	3865		−5.23	−1.03	7	Travertine
SL103B	Modern carbonate	Pasto Chico	23.60313	66.43287	3751		3.39	−7.04	0	Biocarbonate
SL103D	Modern carbonate	Pasto Chico	23.60313	66.43287	3751		3.17	−4.45	0	Biocarbonate
SL103E	Modern carbonate	Pasto Chico	23.60313	66.43287	3751		−3.68	−4.15	0	Biocarbonate
SL53	Palo Pintado Fm.	Angastaco Basin	25.67815	66.09182	1835		−10.30	−6.21	7	Soil carbonate
SL54	Palo Pintado Fm.	Angastaco Basin	25.67815	66.09182	1835		−8.44	−5.39	7	Soil carbonate
SL100	Blanca Lila Fm.	Pasto Chico	24.52308	66.71008	3797		−5.80	−3.81	1	Marl

(*Continued*)

TABLE 1. STABLE ISOTOPIC RESULTS FROM CARBONATES (*Continued*)

Samples	Formation	Location	Latitude (°S)	Longitude (°W)	Elevation (m)	Local thickness (m)	$\delta^{13}C$ (‰, PDB)	$\delta^{18}O$ (‰, PDB)	Age (Ma)	Material
SL102	Blanca Lila Fm.	Pasto Chico	24.24771	66.36310	3836		2.44	−9.33	1	Travertine
SL109	Yacoraite Fm.	Purmamarca	23.70706	65.53575	2628		0.40	1.87	65	Stromatolite
SL 109 S1	Yacoraite Fm.	Purmamarca	23.70706	65.53575	2628		1.00	5.18	65	Stromatolite
SL-109–S2	Yacoraite Fm.	Purmamarca	23.70706	65.53575	2628		0.71	4.16	65	Stromatolite
SL 109 M1	Yacoraite Fm.	Purmamarca	23.70706	65.53575	2628		0.69	1.29	65	Micrite
SL 109 S3	Yacoraite Fm.	Purmamarca	23.70706	65.53575	2628		1.00	2.55	65	Stromatolite
SL 109 M2	Yacoraite Fm.	Purmamarca	23.70706	65.53575	2628		0.40	0.46	65	Micrite
SL 109 OOLITE1	Yacoraite Fm.	Purmamarca	23.70706	65.53575	2628		1.07	1.02	65	Oolite
SL 109 M3	Yacoraite Fm.	Purmamarca	23.70706	65.53575	2628		0.76	−4.40	65	Micrite
SL 109 OOLITE 2	Yacoraite Fm.	Purmamarca	23.70706	65.53575	2628		0.29	0.73	65	Oolite

Note: PDB—Peedee belemnite.

TABLE 2. SUMMARY OF CLUMPED ISOTOPIC DATA FOR YACORAITE (MAASTRICHTIAN) AND MEALLA (PALEOCENE) FORMATION SAMPLES

Sample	Δ_{47} (‰, Caltech)	±1 SE (‰, analytical)	Δ_{47} (‰, ARF)	$T(\Delta_{47})$ (°C, ARF, Ghosh)	$T(\Delta_{47})$ (°C, ARF, D&S)	$\delta^{13}C$ (‰, measured)	$\delta^{18}O_{carb}$ (‰, measured)	$\delta^{18}O_{H_2O}$ (‰), calc. (ARF, Ghosh)	$\delta^{18}O_{H_2O}$ (‰), calc. (ARF, D&S)
Soil carbonate, Mealla Formation (Obelisco)									
SL45B	0.601	0.008	0.650	39	45	−8.79	−5.65	−0.6	0.5
SL47	0.510	0.011	0.556	64	97	−7.90	−5.81	3.6	8.3
SL45c	0.594	0.010	0.643	40	48	−8.81	−5.57	−0.3	1.1
SL46	0.415	0.009	0.459	97	193	−7.64	−5.58	8.6	18.8
SL44a	0.584	0.011	0.632	43	53	−5.85	−3.17	2.7	4.4
SL44c	0.505	0.010	0.551	65	101	−1.80	−8.35	1.1	6.3
Marine/lacustrine carbonate, Yacoraite Formation									
SL109M1	0.564	0.011	0.612	48	63	0.77	1.37	8.1	10.6
SL109M2	0.568	0.008	0.615	47	61	0.49	−0.53	6.0	8.4
SL109S	0.564	0.009	0.611	48	64	0.59	3.07	9.8	12.5

Note: All samples were reacted at 90 °C, with 0.081‰ acid digestion correction. $\delta^{18}O_{H_2O}$ was calculated using values from Kim and O'Neil (1997) for calcite. Analytical precisions are reported for analysis of a single sample aliquot. Precision in $\delta^{18}O$ is 0.02‰ and 0.01‰ or better (1 s.d.). Transfer function from Caltech reference frame to absolute reference frame: $\Delta_{47,}$ARF = 1.0292 (D47, Caltech) + 0.0312 (R^2 = 0.9995). Long-term s.d. in Δ_{47} for standards over the analytical session is 0.009‰ to 0.012‰ (Carrara Marble), on par with the analytical precision of the samples. ARF—absolute reference frame; Ghosh—Ghosh et al., 2006b; D&S—Dennis and Shrag, 2010.

TABLE 3. DEUTERIUM ISOTOPE ANALYSES AND ASSOCIATED PALEOELEVATION RECONSTRUCTIONS FROM VOLCANIC GLASS

Sample no.	Modern elevation (m)	Latitude (°S)	Longitude (°W)	δD glass analysis 1 (‰)	δD glass analysis 2 (‰)	δD glass average (‰)	δD water average (‰)	Age (Ma)	Paleo-elevation* (m) linear	Paleo-elevation* (m) polynomial	Paleo-elevation† (m) polynomial	Tuff or formation
Eastern Andes												
SL-84	3945	24.67255	66.65714	-110	-113	-111	-81	5	4958	4512	4401	Tuff, lower Sijes Fm.
SL-36A	3621	23.40156	66.35854	-98	-98	-98	-67	8	4069	3986	4081	Tuff, Susques
SL-42A	1408	25.85466	65.70324	-69	-66	-67	-35	0.01	1965	2057	2118	Tuff, Holocene
SL-51	1805	25.69376	66.03663	-61	-61	-61	-29	7	1523	1529	1489	Tuff, Palo Pintado Fm.
SL-51	1805	25.69376	66.03663	-64	-61	-62	-29	7	1576	1595	1569	Tuff, Palo Pintado Fm.
SL-22	3051	24.45889	65.93869	-87	-86	-86	-55	0.01	3263	3362	3530	Tuff, Holocene
SL-38	4041	23.99760	66.50781	-111	-113	-112	-82	0.3	5027	4545	4413	Tuzgle ignimbrite
SL-57	1311	25.71498	65.70011	-49	-53	-51	-19	0.01	855	651	398	Tuff, Holocene
SL-58	2773	24.49417	65.88216	-66	-70	-68	-36	0.01	1983	2078	2142	Tuff, Holocene
SL-41	3866	24.22840	66.50781	-117	-116	-116	-86	7.3	5317	4675	4444	Tuff, San Antonio de los Cobres
SL-38	4041	23.99760	66.50781	-109	-114	-111	-81	0.3	4958	4512	4401	Tuzgle ignimbrite
SL-86	3975	24.67596	66.65868	-123	-125	-124	-94	5	5824	4857	4420	Tuff, lower Sijes Fm.
SL-84	3945	24.67255	66.65714	-110	-113	-111	-81	5	4958	4512	4401	Tuff, lower Sijes Fm.
SL-88	4013	24.67596	66.66057	-108	-110	-109	-79	5	4833	4448	4374	Tuff, lower Sijes Fm.
SL-55	1819	25.68088	66.07773	-78	-75	-76	-44	7	2565	2706	2851	Tuff, Palo Pintado Fm.
SL-97	3839	24.69528	66.70174	-99	-102	-101	-70	7	4258	4113	4174	Tuff, upper Pozuelos Fm.
SL-110	1872	27.22685	66.92015	-92	-94	-93	-62	6.7	3723	3736	3875	Tuff, Corral Quemado
SL-112	3028	26.49480	67.40940	-95		-95	-64	0.55	3857	3836	3960	Campo de Piedra Pumice
SL-115	3423	26.12967	67.41487	-59		-59	-27	0.001	1393	1366	1291	Young tuff, Laguna volcano
SL-117	3461	26.51837	67.70420	-75	-73	-74	-42	0.2	2394	2529	2655	Blanca Ignimbrite
SL-118	3417	26.05197	67.42115	-70	-68	-69	-37	2	2077	2185	2265	Galán Ignimbrite
SL-119	4501	25.97513	67.21388	-89	-91	-90	-59	2	3497	3558	3716	Galán Ignimbrite
SL-120	4473	25.97557	67.21407	-79	-83	-81	-49	5	2870	3006	3171	Tuff, Real Grande
SL-121	4339	25.97918	67.21622	-84	-84	-84	-53	5.6	3105	3222	3392	Tuff, lower Merihuaca
SL-122	4302	0.00000	0.00000	-110	-115	-112	-82	6	5054	4558	4417	Blanco Ignimbrite
SL-124	3492	25.99822	67.38950	-92	-86	-89	-58	0.01	3469	3535	3694	Young unnamed tuff
PVN226	3660			-84		-84	-53	7.88	3106	3224	3394	Unnamed tuff
PVN260	3663			-95		-95	-64	7.77	3856	3835	3960	Unnamed tuff
PVN123	3643			-104		-104	-73	9.90	4475	4248	4265	Unnamed tuff
AT2-007	1867			-73		-73	-42	4.81	2374	2508	2633	Unnamed tuff
VV-01	1400			-75		-75	-43	6.35	2463	2602	2736	Unnamed tuff
AT4-003	1847			-76		-76	-45	5.17	2589	2730	2877	Unnamed tuff
AT6-001	1890			-95		-95	-64	4.61	3843	3826	3952	Unnamed tuff
AT4-001	1820			-74		-74	-42	6.90	2390	2525	2651	Unnamed tuff
AT7-010	1857			-85		-85	-54	5.98	3188	3296	3466	Unnamed tuff
AT1-001a	1984			-75		-75	-43	7.24	2489	2628	2765	Unnamed tuff
AT3-009	1822			-75		-75	-43	4.04	2475	2614	2749	Unnamed tuff
LVT1-006	1200			-78		-78	-46		2660	2801	2954	Unnamed tuff

(*Continued*)

TABLE 3. DEUTERIUM ISOTOPE ANALYSES AND ASSOCIATED PALEOELEVATION RECONSTRUCTIONS FROM VOLCANIC GLASS (Continued)

Sample no.	Modern elevation (m)	Latitude (°S)	Longitude (°W)	δD glass analysis 1 (‰)	δD glass analysis 2 (‰)	δD glass average (‰)	δD water average (‰)	Age (Ma)	Paleo-elevation* (m) linear	Paleo-elevation* (m) polynomial	Paleo-elevation† (m) polynomial	Tuff or formation
Salar de Arizaro Basin												
A09-I-1	3737			−94	−91	−92	−61	5	3671	3696	3840	Unnamed tuff
A09-I-2	3559			−89	−95	−92	−61	34.8	3641	3673	3820	Unnamed tuff
ARB09-4	3807			−77	−72	−75	−43	1	2456	2594	2728	Unnamed tuff
ARB09-7	3782			−92	−86	−89	−57	1	3416	3491	3654	Unnamed tuff
ARB09-9	3833			−82	−82	−82	−50	0.4	2948	3079	3246	Unnamed tuff
ARB09-2	4140			−94	−95	−94	−63	18.8	3821	3809	3938	Unnamed tuff
ARB09-1	3827			−89	−90	−90	−59	19.5	3496	3557	3715	Unnamed tuff
ARB09-14	4185			−86	−102	−94	−63	17.9	3804	3797	3928	Unnamed tuff
ARB09-6	3763			−98	−97	−98	−67	13.9	4058	3979	4075	Unnamed tuff
ARB09-8	3821			−88	−90	−89	−57	15.8	3422	3496	3658	Unnamed tuff
Salar de Fraile Basin												
1SF49	3400	25.89020	68.09000	−102	—	−102	−71	38.5	4327	4157	4205	Tuff, Quinoas I Formation
5SF128	3522	25.89020	68.09000	−124	—	−124	−94	34.8	5841	4862	4418	Tuff, Quinoas I Formation
5SF257.5	3550	25.89020	68.09000	−103	—	−103	−72	33.2	4404	4205	4237	Tuff, Quinoas I Formation
5SF362	3564	25.89020	68.09000	−105	—	−105	−74	32.9	4541	4287	4288	Tuff, Quinoas I Formation
6SF128	3593	25.89020	68.09000	−124	—	−124	−94	31.1	5841	4862	4418	Tuff, Quinoas II Formation
6SF148	3600	25.89020	68.09000	−96	—	−96	−65	32.2	3952	3905	4017	Tuff, Quinoas II Formation
6SF284	3650	25.89020	68.09000	−116	—	−116	−86	31	5294	4665	4442	Tuff, Quinoas II Formation
6SF479	3675	25.89020	68.09000	−91	—	−91	−60	29.8	3576	3621	3773	Tuff, Quinoas II Formation
6SF664	3708	25.89020	68.09000	−102	—	−102	−71	24.2	4322	4154	4203	Tuff, Chacras Fm.
6SF753	3750	25.89020	68.09000	−142	—	−142	−113	23.3	7073	5067	3942	Tuff, Chacras Fm.
7SF9	3813	25.89020	68.09000	−122	−120	−121	−91	19.2	5629	4794	4441	Tuff, Portrero Grande Fm.

*This paper.
†Canavan et al. (2014).

[204]Hg and [204]Pb), and because very little Hg was present in the argon gas. Additional details about analytical procedures are described by Gehrels et al. (2008).

Interelement fractionation of Pb/U is generally ~15%, whereas fractionation of Pb isotopes is generally <2%. In-run analysis of fragments of a large zircon crystal (every sixth measurement) with known age of 563.5 ± 3.2 Ma (2σ error; Gehrels et al., 2008) was used to correct for this fractionation. Fractionation also increases with depth into the laser pit by up to 5%. This depth-related fractionation was accounted for by monitoring the fractionation observed in the standards. Analyses that displayed >10% change in ratio during the 20 s measurement were interpreted to be variable in age (or perhaps compromised by fractures or inclusions) and are excluded from further consideration. Also excluded are analyses that yielded >15% uncertainties in [206]Pb/[238]U ages or were >5% reverse discordant.

The measured ages of 12 tuff samples are reported in Table 4, with errors reported at the 2σ level. Ages for each sample are defined by analysis of 4–28 grains.

PALEOALTIMETRY

Isotopic Results and Implications from Carbonates

Carbonates were sampled from a variety of formations spanning most of the Cenozoic (Table 1; Fig. 4). The oldest of these come from the Maastrichtian–Paleocene (Danian) Yacoraite Formation of the Balbuena Group. Younger samples come from the Paleocene Mealla Formation and Paleocene–Eocene Maiz Gordo Formations of the Santa Bárbara Subgroup, and the overlying Eocene–Oligocene Quebrada de los Colorados Formation of the Metán Group. Here, we present $\delta^{18}O$, $\delta^{13}C$, and Δ_{47} results

TABLE 4. U-Pb (ZIRCON) GEOCHRONOLOGIC ANALYSES BY LASER-ABLATION–MULTICOLLECTOR–INDUCTIVELY COUPLED PLASMA–MASS SPECTROMETRY

Sample	No. of grains	Weighted mean age (Ma)	±2σ (%)	MSWD
1SF49	22	38.5	0.7 (1.8)	0.4
5SF128	18	34.7	0.7 (2.0)	0.2
5SF257.5	8	33.3	1.4 (4.3)	0.2
5SF362	11	32.9	2.9 (8.7)	0.1
6SF128	23	31.1	0.9 (2.8)	0.2
6SF148	4	32.3	2.5 (7.7)	0
6SF284	23	31	0.8 (2.6)	0.2
6SF479	20	29.8	0.3 (1.0)	6.7
6SF664	10	24.2	0.9 (3.5)	4.2
6SF753	11	23.3	1 (4.4)	0.1
7SF9	19	19.2	0.6 (3.1)	0.3
SL-122	28	5.8	0.1 (2.2)	9.7

Note: MSWD—mean square of weighted deviates.

from the carbonates, mostly from paleosols. Where unaltered by burial, $\delta^{18}O$ values from all carbonates provide information on paleoelevation and local climate; $\delta^{13}C$ values from paleosols relate directly to the nature of vegetation cover; and Δ_{47} results yield surface paleotemperatures, which in turn can provide estimates of paleoelevation.

Balbuena Subgroup

Micrites, stromatolites, and oolites ($n = 9$) from the Yacoraite Formation (Fig. 2) sampled near Purmamarca (Fig. 1) yielded $\delta^{13}C$ (VPDB) values of +0.7‰ ± 0.3‰ and $\delta^{18}O$ (VPDB) values of +1.4‰ ± 2.7‰ (Table 1; Fig. 4). These results are in line with most values previously obtained for the Yacoraite Formation from a broad area of northwestern Argentina (Marquillas et al., 2007).

The Yacoraite Formation is the oldest and most deeply buried of the formations we studied and is therefore the most likely to have been modified by diagenetic resetting. The positive isotopic values for both carbon and oxygen, however, strongly argue against resetting of either system. Results are consistent with a marine or low-elevation lacustrine setting for the Yacoraite for this time period, although the $\delta^{18}O$ (VPDB) values are on the high side of typical marine averages for this time period (Veizer et al., 1999). The origin of the Yacoraite has been the focus of much discussion (Palma, 2000; Marquillas et al., 2007), and it appears that the Yacoraite Formation is both marine and lacustrine. Even if entirely lacustrine in origin, the elevated $\delta^{18}O$ values of the Yacoraite are very difficult to explain by diagenetic resetting at higher temperatures, which tends to decrease $\delta^{18}O$ values.

The three Yacoraite Formation samples analyzed for Δ_{47} paleothermometry yielded indistinguishable, warmer than Earth-surface temperatures (*T*), of 47–48 °C (or 61–64 °C using Dennis et al., 2011; Table 2 herein). These warm temperatures suggest that the samples underwent some degree of diagenetic "resetting." Resetting could be due to diffusion of carbon and oxygen through the mineral lattice (Passey and Henkes, 2012) or to recrystallization, although carbonates from the Yacoraite and from paleosols in overlying foreland formations appear to remain largely unaltered and micritic, arguing against wholesale recrystallization and secondary introduction of cements. Quade et al. (2013) documented such resetting of Miocene-age carbonates from Nepal and Pakistan when buried >3–4 km (or >125 °C), and burial temperatures of ~100 °C or higher can cause solid-state C-O bond reordering (Henkes et al., 2014). The Yacoraite was overlain by 2–6 km of younger foreland deposits in the region (Carrapa et al., 2011a; DeCelles et al., 2011), and so deep burial could account for the resetting. Although resetting due to diffusive reordering of C-O bonds or cryptic recrystallization has obscured any primary paleotemperature information in these samples, the positive bulk $\delta^{13}C$ (VPDB) and $\delta^{18}O$ (VPDB) values do not appear to be altered by this process.

If our interpretation is correct, then higher than Earth-surface $T(\Delta_{47})$ values cannot necessarily be used to screen for diagenetic alteration of the bulk isotopic composition of samples if the $T(\Delta_{47})$ values reflect diffusive reordering or recrystallization in a
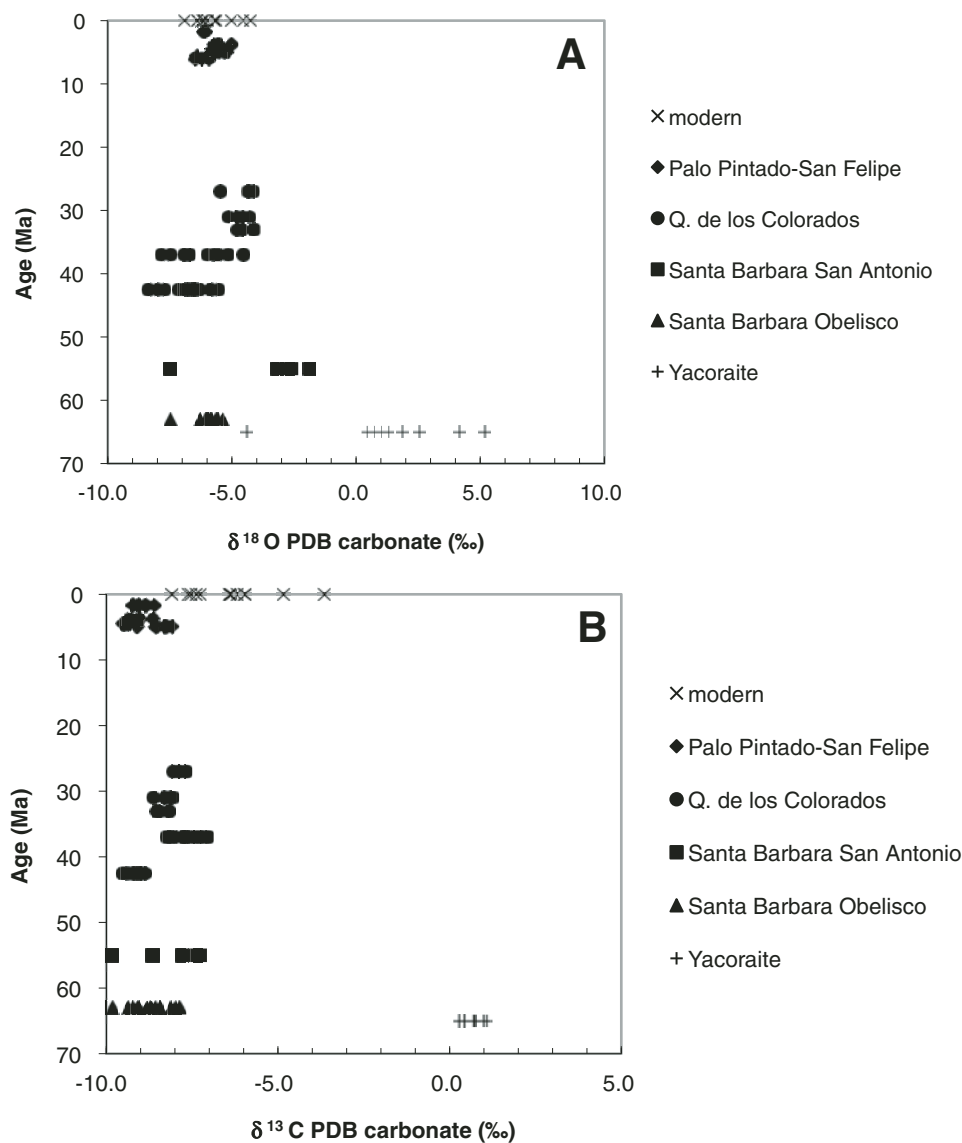
The growth of the central Andes, 22°S–26°S

Figure 4. (A) $\delta^{18}O$ values and (B) $\delta^{13}C$ values of carbonates from Late Cretaceous to recent carbonates from areas now exposed in the easternmost Puna, Eastern Cordillera, and Subandes, 22°S–26°S (see Fig. 1 for locations). PDB—Peedee belemnite.

rock-buffered system (e.g., Huntington et al., in press). Moreover, although $\delta^{18}O$ values of water can be calculated using the $T(\Delta_{47})$ and $\delta^{18}O$ values of carbonate from the same sample (Table 2), such values will be difficult to interpret if the $T(\Delta_{47})$ value reflects diffusive reordering rather than the temperature of calcite crystallization from either Earth-surface or diagenetic waters.

Santa Bárbara and Metán Subgroups

Pedogenic carbonate isotopic values from Vertisols or reworked from Vertisols and Calcisols in the Mealla and Maiz Gordo Formations of the Santa Bárbara Subgroup (Fig. 2), and from the overlying Quebrada de los Colorados Formation of the Metán Subgroup are very similar and fall mostly in the −8‰ to −9‰ range for $\delta^{13}C$ (VPDB) and −4‰ to −6‰ for $\delta^{18}O$ (VPDB) (Fig. 4; Table 1).

These $\delta^{13}C$ (VPDB) values are consistent with soils that were covered by dominantly C_3 plants respiring at moderate to high rates (Fig. 4; Cerling and Quade, 1993; Quade et al., 2007). The C_3 cover is consistent with the absence or rarity of C_4 plants globally before the Miocene. The high soil respiration rates suggest semiarid to subhumid conditions, which typify elevations <1000 m in the region today. It is highly inconsistent with the desolate, nearly plantless setting of the >3000-m-high Andes. This holds for both the modern and the past, based on the extensive evaporites in partially age-equivalent deposits of the Quiñoas Formation at Salar de Fraile, discussed in the Evaporites and Paleoaltimetry section.

The consistently high $\delta^{18}O$ values of these formations also point to low paleoelevations of <1000 m (Fig. 5), entirely consistent with the foredeep to back-bulge foreland settings
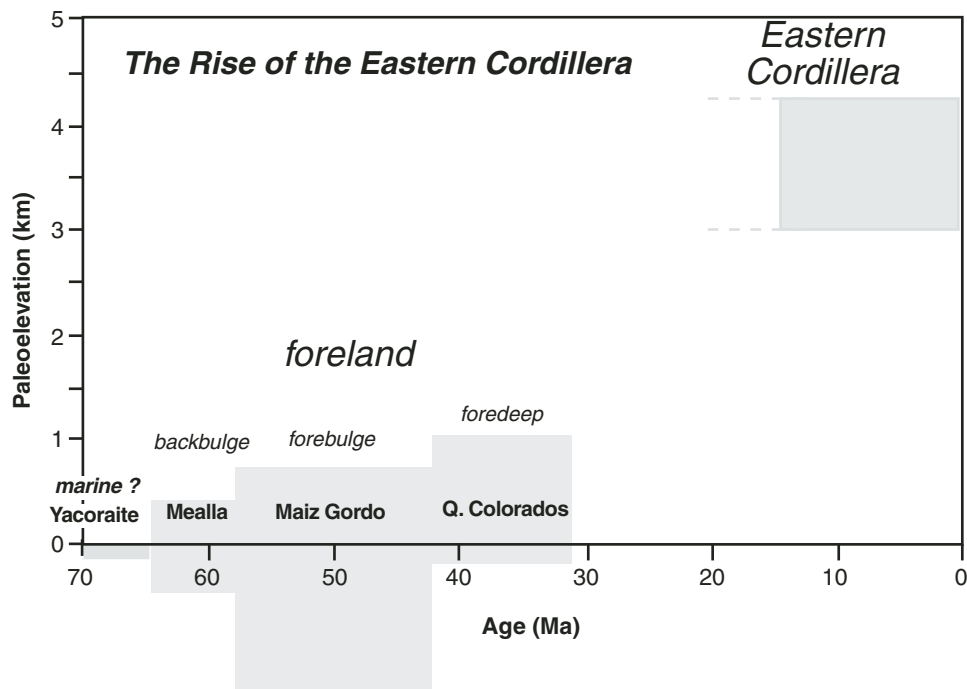
Figure 5. Uplift of the Eastern Cordillera region during the Cenozoic, based on oxygen isotopic results from carbonates, deuterium isotope values from volcanic glass, and the distribution of evaporites.

envisioned for the Santa Bárbara and Metán Subgroup deposits (DeCelles et al., 2011). For comparison, modern elevations in the Andean foreland basin system range from near sea level in the far east to ~400 m in the proximal foredeep and wedge-top depozones. They are also consistent with values from modern low-elevation carbonates sampled in Quebrada del Toro (Table 1; Fig. 1). We regard this comparison as valid even though Paleogene climate was warmer and the $\delta^{18}O$ value of the ocean was slightly lower. This region has probably always been embedded in the subtropical easterlies, which provides a probable reason why large departures from the present are not visible isotopically.

The Santa Bárbara and Metán Subgoup paleosol carbonates give a wide range of $T(\Delta_{47})$ values, most of which are too high for primary soil temperatures (Quade et al., 2013) and point to some diagenetic resetting (Table 2). Like the Yacoraite Formation carbonates, these samples were buried to 2–6 km. Four of the samples have similar $\delta^{18}O$ and $\delta^{13}C$ of carbonate values (around −6‰ and −8 ‰, respectively) but very different $T(\Delta_{47})$ values, ranging from 39 °C to 97 °C (or 45–193 °C using Dennis et al., 2011). The other two samples vary in their $\delta^{18}O$ and $\delta^{13}C$ carbonate values, but their temperatures fall within the large temperature range of the other paleosol carbonate samples. The fact that $\delta^{18}O$ and $\delta^{13}C$ values appear consistent among samples with highly variable $T(\Delta_{47})$ values strongly suggests that the bulk isotopic composition has remained primary while diffusive C-O bond reordering or cryptic recrystallization has occurred to varying extents among the samples. As a result, reconstruction of $\delta^{18}O$ of water values calculated from the $T(\Delta_{47})$ and $\delta^{18}O$ of carbonate data would be misleading.

Bywater-Reyes et al. (2010) studied a thick Neogene-age sequence of basin-fill deposits now in the eastern part of the Eastern Cordillera near the village of Angastaco. They reported $\delta^{18}O$ (VPDB) values from paleosol carbonates in the Palo Pintado (9–5 Ma) and San Felipe Formations (5–2 Ma) of −5.8‰ ± 0.5‰ ($n = 35$). This range excludes some results from the bottom of the section that appear not to be paleosol carbonate due to their low $\delta^{13}C$ values (<–14‰; figure 2 *in* Bywater-Reyes et al., 2010).

The Angastaco area deposits today are moderately elevated at ~2 km. Carrapa et al. (2011a) interpreted the Palo Pintado Formation as wedge-top deposits and the San Felipe Formation as intermontane paleovalley deposits (Fig. 2). The elevated $\delta^{18}O$ (VPDB) values in these formations point to a paleoelevation of ≤1 km. Paleosol carbonate $T(\Delta_{47})$ measurements averaging 24 ± 4 °C ($n = 9$; 1 s.d.) and as warm as 32 °C also suggest low paleoelevations (Carrapa et al., 2014b).

Carbonates are rare in younger deposits in the now high Puna Plateau. These are confined to a few carbonates in lake deposits otherwise dominated by clastic sediments or evaporites. The $\delta^{18}O$ values in these carbonates tend to be high and variable at −1.4‰ ± 3.2‰ (Table 1). These high values were likely produced by evaporation from shallow lakes and salt pans. The rare paleosols in these deposits are gypsiferous and lack carbonate, a characteristic of soils of the modern hyperarid Atacama (Quade et al., 2007). Relatively cool paleosol carbonate temperatures indicated by two $T(\Delta_{47})$ measurements are ~15 °C, suggesting higher elevations than the Angastaco area samples (Carrapa et al., 2014b). Taken together, conditions on the Puna Plateau were clearly arid to hyperarid and likely at high elevation since at least 10 Ma.

Isotopic Results and Implications from Volcanic Glass

More than 30 tuffs with preserved volcanic glass were analyzed for δD composition in this study (Table 3). Almost all come from >3000 m elevation in the Puna and Eastern Cordillera. Some tuffs were previously dated by other studies, whereas others were dated for this study using zircon U-Pb geochronology (Table 4). The samples that we report here range in age from 38 to 2 Ma. The δD (SMOW) values for the glass range from −73‰ to −142‰ (Table 3).

We reconstruct ancient water values (Table 2) using a water-glass fractionation factor ($\alpha_{\text{water-glass}}$) of 1.0342, which Friedman et al. (1993) established experimentally, and confirmed empirically. Dettinger and Quade (this volume) studied the δD composition of modern water and Quaternary-age glass in the eastern Andes. They observed a similar 30‰–35‰ fractionation between the δD values of water and glass across a range of elevations, supporting Friedman's conclusions.

Dettinger and Quade (this volume) sampled modern water across a wide elevation range and determined the following relationship for the Eastern Cordillera:

$$\text{elevation (m)} = -66.2 \times (\delta D_{\text{water}}) - 375.3 \ (r^2 = 0.90, n = 25). \ (1)$$

In the western part of the Puna, δD_{water} values increase less rapidly with elevation, and a polynomial fit to the combined Eastern Cordillera and Puna data is:

$$\text{elevation (m)} = -0.4775 \times (\delta D_{\text{water}})^2 - 109.63(\delta D_{\text{water}}) - \quad (2)$$
$$1222.8 \ (r^2 = 0.90, n = 29).$$

The δD values of 2–0 Ma glass also from the Eastern Cordillera display the same slope as Equation 1 but are offset by 30‰–35‰, supporting the idea that our modern water sampling is representative of long-term $\delta D_{\text{water-elevation}}$ relationships.

Potential Complications

Considerable uncertainty attends any use of such modern relationships to reconstruct paleoelevation, chief among them the effects of climate change. This can be partly redressed by comparing ancient lowland samples to modern archives at low elevation, in order to discern net climate-driven changes in isotopic compositions of known elevation. Differences between ancient and modern archives of similar elevation equate to climate change, which presumably influences both low- and high-elevation records. We therefore correct for the effects of climate change by comparing carbonates from the Eocene–Oligocene Quebrada de los Colorados Formation to Quaternary carbonates. The $\delta^{18}O$ (VPDB) values of carbonate near sea level from this time period are in the −8‰ to −4‰ range, for an average of around −6‰, very similar to values of Quaternary-age carbonate (Fig. 4). The isotopic range probably arises from variable evaporation of soil water, perhaps coupled with some contribution to soil nodules composition by groundwater fed from higher elevations, since

many of the foreland soils show hydromorphic features. Evidently, climate change in this region during the Cenozoic did not appreciably alter the isotopic composition of lowland rainfall. Moreover, we can safely assume that changes in continentality in the Andes had little effect on the isotopic composition of rainfall over the Cenozoic. For example, the distance that moisture must travel over land via the NE trades, now and in the past, is 2000–3000 km, which is much larger than any changes due to tectonic shortening (~150 km) of the orogen. Therefore, climate change and tectonic shortening of Andes likely played a minimal role in altering the isotopic composition of meteoric water across all elevations.

Another key question is how the slope of Equations 1 and 2 may have differed in the past. Ehlers and Poulsen (2009) have suggested that slopes were less steep in the past when the Andes as a whole were lower, i.e., less change in isotopic compositions for a given change in elevation. In this view, the isotopic gradients only attained their present steepness once the bulk of the Andes, rising en masse, crossed a certain threshold. If correct, our reconstructed paleoelevations described in the next section using Equations 1 and 2 are minima.

However, we argue that isotopic gradients up the east face of the paleo-Andes and onto the Puna probably did not differ appreciably from today because the geologic evidence (see Ancient Evaporites and Paleoelevation section) points to high elevations already in place in the Puna by 38 Ma. Modeling predicts that the dry climate of the pre-uplift Andes should have produced high (>+3‰) $\delta^{18}O$ (SMOW) values for rainfall (Ehlers and Poulsen, 2009). Our results are uniformly more negative (<–5‰) for all formations back to the Paleocene, arguing for the presence of elevated uplands through nearly all the Cenozoic. In our view, the only changes have been that the east-bounding topographic front stepped eastward with time. If correct, isotopic gradients should not have appreciably changed.

Western Puna Plateau: Salars de Fraile and Arizaro

Using δD values from glass (Table 3), we can reconstruct the paleoaltimetric evolution of the region through time, bearing in mind the assumptions just described. Eocene- and Oligocene-age tuffs from two large hinterland basins in the western Puna (Fig. 1), the Fraile and Arizaro Basins, span the entire period roughly 40 Ma to present. Glass from 10 tuffs in the Fraile Basin yielded average δD values of −120‰ ± 14‰ (1σ), and water δD values of −90‰ ± 14‰ using the water-glass fractionation factor from Friedman et al. (1993). U-Pb dating of zircons from some of these tuffs reveals an age that ranges from 38.4 to 19.2 Ma (Table 4). Ten additional tuffs from the Arizaro Basin (21.5–1 Ma; Boyd, 2010; DeCelles et al., this volume) yielded average glass δD values of −89‰ ± 7‰ and average reconstructed water δD values of −58‰ ± 7‰ (Canavan et al., 2014).

Using Equation 2, these isotopic results translate into paleoelevations of 4100–5100 m for the Fraile glasses, and 2600–4000 m for the Arizaro glasses (Fig. 6). Use of Equation 1 yields even higher paleoelevations, but we regard Equation 2
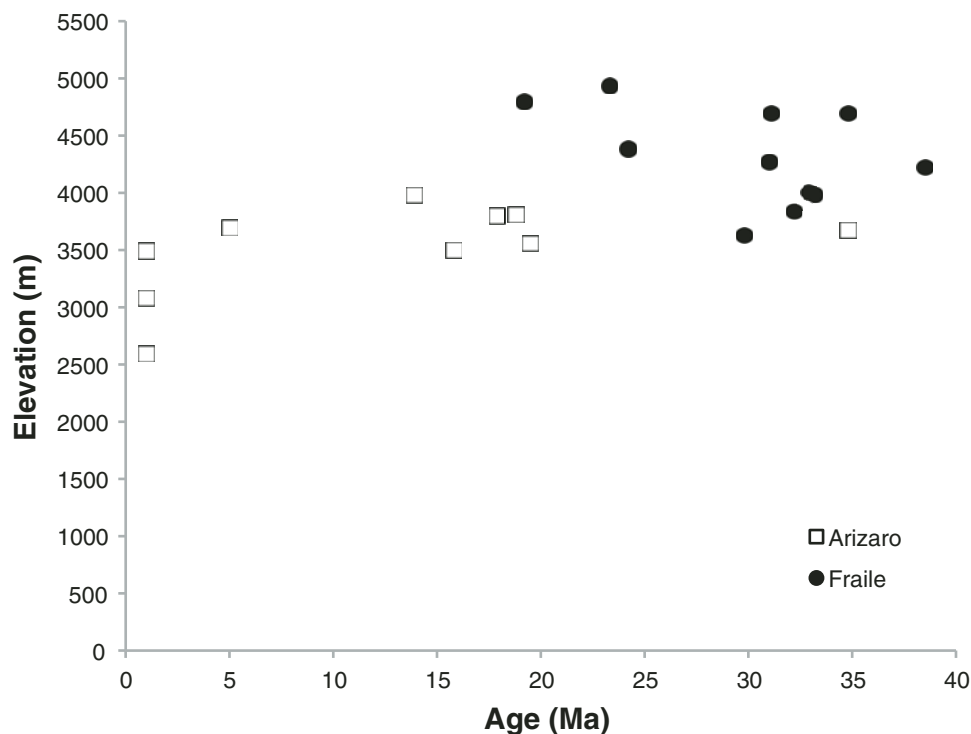
Figure 6. Paleoelevation reconstruction for 22°S–26°S based on the δD value of glass from the Fraile and Arizaro areas of the Puna Plateau (see Fig. 1). The modern elevation of these Puna basins is 3500–4000 m.

as more appropriate, because it includes natural waters from the Eastern Cordillera and Puna. As already noted, no correction for climate change was made, because the δ18O value of lowland soil carbonates contemporaneous with the Fraile and Arizaro tuffs does not differ appreciably from the modern values. The modern elevation of the Fraile and Arizaro deposits is 3500–4200 m. Hence, paleoelevations since the late Eocene have been at least as high as the present. A few of the youngest (<5 Ma; Fig. 6) samples from Arizaro appear to mark a recent drop in elevation for that basin, not inconsistent with the evidence for late Neogene extension and normal faulting (Schoenbohm and Carrapa, 2011).

Our paleoelevation results, which are based on empirically derived models, can be compared to the results of Canavan et al. (2014), who used a theoretical model (Rowley and Garzione, 2007) to estimate paleoelevations of the Puna. Using this fairly different approach based on atmospheric thermodynamics and the process of Raleigh distillation during orographic uplift, Canavan et al. (2014) produced modeled paleoelevations for the Puna Plateau from 38 Ma to recent, also based on δD of volcanic glass samples (including samples from the Fraile and Arizaro Basins). The paleoelevation estimates made by Canavan et al. (2014) average ~1–0.5 km lower in elevation than ours but tell a similar story of an already elevated Puna Plateau (at least 2.5–3.5 km) by the late Eocene.

Eastern Andes

We analyzed δD values of glass from 22 tuffs and ignimbrites (Table 3) in the eastern portion of the Andes. They range in age from near-modern to 8 Ma and include glass from some of the Altiplano-Puna volcanic complex eruptions and other large ignimbrites, including Cerro Galán and Tuzgle (Fig. 1). The oldest of these samples yielded paleoelevations between 4000 and 4700 m, somewhat higher than elevations of the samples today at 3600–3900 m. This suggests that much of the Eastern Cordillera and eastern Puna Plateau had attained near-modern elevation by the late Miocene (Fig. 5).

The δD analyses of glass from two tuffs sampled by the first author (Quade) from the Palo Pintado Formation (9–5 Ma) in the Angastaco area (Fig. 1) indicate paleoelevations of ~1.5 km (Table 3). The modern sample elevation is 1.8 km, suggesting that the Angastaco area was modestly elevated while accommodating sediment during the late Miocene. As previously discussed in the section on carbonates, Carrapa et al. (2011a) placed the Palo Pintado Formation in the wedge-top depozone. These data are consistent with other paleoelevation proxies (δD, Δ_{47}) from the Eastern Cordillera, which, combined with geological evidence, indicate that the Angastaco Basin and areas to the east (La Vina) had attained their modern elevation during the mid-Miocene (Carrapa et al., this volume).

EVAPORITES AND PALEOALTIMETRY

Modern Salt Evaporite Distribution

Evaporites are common in the geologic record of the central Andes. They provide information not only about paleoclimate and orography, following Vandervoort et al. (1995), but we suggest also paleoaltimetry. The modern distribution of

saline lakes in South America provides a vital perspective on their interpretation.

Saline lakes are found along almost the entire length of South America south of 10°S (Fig. 7). North of this, the climate is generally too wet for saline lakes to develop, the exception being far northeastern Brazil. South of 10°S, modern saline lakes occupy two basic positions, depending on prevailing wind direction. South of ~29°S, all saline lakes are east of the Andes. Prevailing
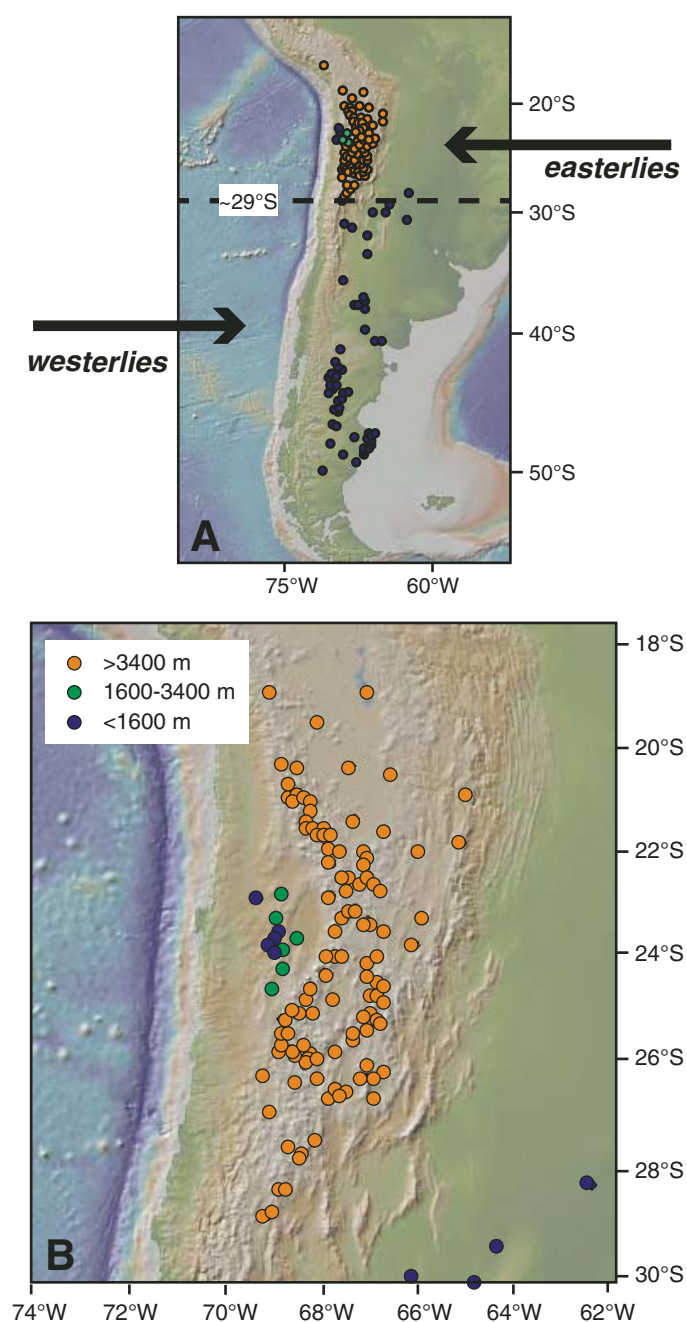

Figure 7. Distribution of salt pans in South America >1 km in diameter by elevation: (A) all of southern South America, with prevailing winds indicated, and (B) the subtropics of South America north of 30°S.

winds at these latitudes are westerly, and the moisture they bear is blocked by the Andes (Fig. 7A). What little rain penetrates the Andean rain shadow is carried by easterly intrusions of moist air from the Atlantic. Tectonically, the lakes lie mostly in the fore-deep, back-bulge (e.g., Cohen et al., this volume), or in shallow local cratonic and volcanic depressions. They also are confined to elevations of <1600 m, and mostly <1000 m.

Between 29°S and ~10°S, saline lakes take on a completely different distribution and are confined to the high Andes and the Atacama Desert to the west. No dry/saline lakes are present east of the Andes in this latitudinal belt, although lakes are widespread in this region. This is because moisture at these latitudes is born from the Atlantic Ocean by the easterlies. Easterlies are blocked by the high Eastern Cordillera, creating a rain shadow to the west. In the Andes between 10°S and 29°S, the saline lakes are, without exception, at high elevation, >2900 m and mostly >3400 m (Fig. 8). However, in the Atacama Desert, saline/dry lakes range in elevation from 500 to 5500 m.

Between 10°S and 29°S (a latitude range that is the region of focus in this study), the strong relationship between saline lakes and high elevation is due to a combination of aridity and internal drainage on the Puna Plateau. Easterly air masses rise along the steep eastern front of the Andes, cool, and rain out most of their moisture between 0 and 2 km elevation. By 3 km, rainfall averages 20 cm/yr, compared to ~100–300 cm/yr at 500 m elevation at the eastern front of the Andes (Strecker et al., 2007). Evaporation far exceeds precipitation on the Puna Plateau, and a strongly negative moisture balance favors evaporite formation.

Internal basin drainage, of course, is also essential to evaporite development. Many basins on the high Puna Plateau >2900 m are hydrographically closed, whereas basins at lower elevations to the east in the Subandes and Santa Bárbara Ranges are all externally drained. Ranges in the Subandes can be very high (>5000 m) but are not continuous, and easterly moisture passes around and behind them. This effect diminishes with elevation, to the point where drainages in the higher Subandes lose stream power, leading to their eventual hydrographic isolation (Humphrey and Konrad, 2000; Sobel et al., 2003; Strecker et al., 2007). The point at which local drainage changes from external to internal depends on the competing factors of uplift rate, rainfall, and rock erodibility. The whole of the Subandes is undergoing rapid shortening and exhumation (Echavarria et al., 2003; Carrapa et al., 2011b). At <2 km elevation, these tectonic forces that would disrupt and potentially isolate drainage systems are exceeded by the higher rainfall, locally assisted by erodible rocks, thus promoting external drainage. At >2 km, tectonic processes gradually overwhelm diminishing rainfall, and basins cannot maintain external drainage. Internal drainage leading to saline lake formation develops very consistently at elevations >3000 m all along this sector of the eastern Andes.

At the latitudes examined in this study (22°S–26°S), we therefore take the presence of ancient evaporites in basin deposits of the Andes to indicate high paleoelevation (>2900 m, and likely >3400 m), provided certain conditions were met. For this to be
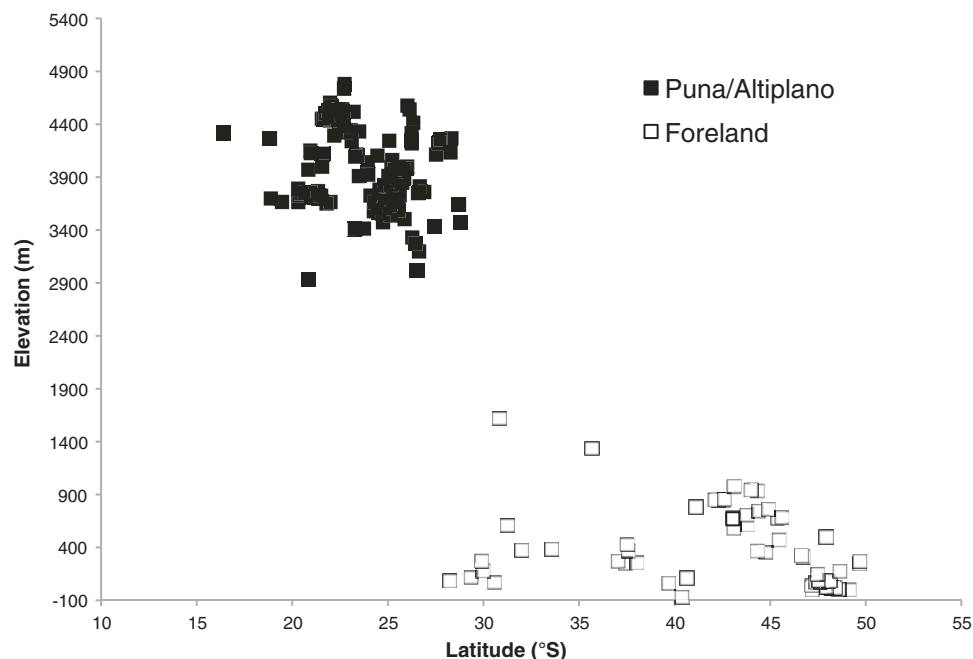
Figure 8. Elevation distribution of salt pans in South America >1 km in diameter, excluding the Atacama Desert. No salt pans are found between 1600 and 2900 m, and most salt pans are confined to >3400 m (all north of 29°S) and <1000 m (all south of <29°S).

true, the easterlies, not the westerlies must have dominated rainfall at this latitude. Had the westerlies dominated, the pattern of salt lakes would be like it is today south of 29°S, where salt lakes abound in the low-elevation foreland, and their presence would not imply high elevations. Second, the paleolatitude of the basin of interest and the transition between easterlies and westerlies must not have changed significantly during the Cenozoic. All indications are that the easterlies were as far south and possibly farther south throughout the Cenozoic, when global climate was warmer and the subtropics more expansive. Moreover, South America has not drifted in latitude appreciably during the Cenozoic.

It is important to be clear that we are making the saline lake–high elevation connection only for the midlatitude Andes between 10°S and 29 °S. Obviously, in other parts of the world, salt lakes occur in low-elevation basins, often in rain shadows, at this and other latitudes. Death Valley, USA, and other internally drained Basin and Range grabens are good examples. There, however, the tectonic setting is extensional, and the basins reside in the lee of the Sierra Nevada and other high ranges that block the moisture-bearing westerlies. The Andes currently are generally contractional, except for areas at the margin of the plateau and in the interior of the Puna, which are characterized by recent localized normal faulting (Schoenbohm and Strecker, 2009; Zhou et al., 2013). Hence, no low-elevation basins are found on the Puna, without exception. This latitude of the Andes has probably been under continuous compression since the cessation of Salta rifting in the Late Cretaceous to Paleocene (Pardo-Casas and Molnar, 1987; Soler and Bonhomme, 1990).

Saline and dry lakes are widespread at a range of elevations in the Atacama Desert west of the Western Cordillera of the Andes. As with Death Valley, salt pans in the Atacama have no implications for paleoelevation, but merely indicate that the Andes to the east were sufficiently elevated to block the easterlies. The discussion that follows is confined to geologic sections that during deposition were east of the coeval Andean magmatic arc—the modern setting for the uniformly high-elevation saline lakes. If our hypothesis—that the present Andes is a key to understanding the paleo-Andes—is correct, then evaporites in the geologic record of the Andes at this latitude indicate paleoelevations >3000 m. This analysis expands upon the observations of Vandervoort et al. (1995), who used evaporite distribution to infer development of orographic blockage of moisture but not necessarily paleoelevation on the eastern Andes during the Neogene.

Ancient Evaporites and Paleoelevation

Evaporites are known from a number of Cenozoic sections in this sector of the Andes (Alonso et al., 1991; Vandervoort et al., 1995), but they are conspicuously absent from age-equivalent deposits in the modern Subandes (Strecker et al., 2007). This is consistent with our view that evaporites—past and present—are confined to elevations >3000 m. Here, we survey the occurrence of evaporites from west to east across the Andes. In general, the age of the oldest evaporites tends to decrease eastward (Fig. 9). Evaporites first appear in Upper Cretaceous strata in the forearc in Chile, in Upper Eocene rocks in the eastern forearc and Puna Plateau, and in mid-Miocene strata in the eastern Andes.

Starting our survey of evaporites in the modern forearc in Chile, the oldest evaporites are exposed in the Cordillera de Domeyko on the western margin of the Salar de Atacama (Hartley et al., 1992; Mpodozis et al., 2005) (Fig. 1). This includes thick evaporites of the Tonel Formation, which is very poorly

dated but thought to be mid- to Late Cretaceous in age. The upper Orange (Naranja) Formation, of Paleocene to early Eocene age, also contains evaporites (Mpodozis et al., 2005; Arriagiada et al., 2006). All these evaporites were deposited to the east of the concurrent magmatic arc, before it stepped eastward after ca. 27 Ma. Again drawing on modern analogs, the presence of evaporites would place this region of the present forearc at high elevations in a retroarc position as far back as the Paleocene to early Eocene, and possibly as far back as the Tonel Formation, whatever its age turns out to be.

Evaporites are also abundant in the Oligocene–Miocene Paciencia Formation, the forerunner of the modern Salar de Atacama. By the mid-Oligocene, the main axis of the magmatic arc had shifted eastward to its current position in the Western Cordillera, and thus the Paciencia Formation was deposited in the forearc. The entire forearc then and today lies in the rain shadow of the lofty Western Cordillera, producing hyperarid conditions. In this setting, evaporites form at a broad range of elevations and provide no constraints on paleoelevation for the period <27 Ma. Since the Salar de Atacama area today lies at 2500 m, we suggest it must have lost 1–2 km of elevation since the Eocene (when it lay in a retroarc setting). Evenstar et al. (2009) and Jordan et al. (2010) documented tilting of surfaces and ignimbrite flows to show that the western slope of the Andes stood ~2000 m above the adjacent forearc (now at ~1–1.5 km) by the early to mid-Miocene, and it has added a further ~1 km since then. Their analysis focused on relief, not paleoelevation, so the surface and ignimbrite tilting evidence could support the idea that relief development was due to both the drop of the Atacama (the forearc) and the rise of the Andes.

Evaporites are extensive in the Andes in sections exposed in the central Puna Plateau and the lee of the Western Cordilleran magmatic arc. At Salar de Fraile, they extend back to Member I of the Quinoas Formation (≥38 Ma; Kraemer et al., 1999; Carrapa et al., 2011b; Table 4). Farther north, on the southwest flank of the modern Salar de Arizaro, the oldest evaporites date to the late Eocene (DeCelles et al., this volume). All these evaporites occur just to the east of the main axis of the contemporaneous magmatic arc of the ancestral Western Cordillera (Trumbull et al., 2006). Hence, these basins resided east of the magmatic arc in the paleo-Puna, and not within the forearc (i.e., Atacama-like setting). As such, we interpret the presence of thick evaporites in these sections to indicate the attainment of >3000 m elevations by the late Eocene in this part of the west-central Andes.

Farther eastward in the Puna Plateau, evaporites have been forming since the middle Miocene and are actively forming today. According to the survey of Vandervoort et al. (1995), the oldest evaporites at ca. 15 Ma are found in the Salar de Hombre Muerto (Fig. 9). Prior to 15 Ma, fluvial red beds as old as 37–39 Ma (DeCelles et al., 2007; Carrapa and DeCelles, 2008), but no evaporites, characterize basin sedimentation. Vandervoort et al. (1995) interpreted ca. 15 Ma to mark blockage of easterly moisture and the development of internal drainage in the area. We agree but go further to say that this is also when paleoelevations in the eastern Puna rose above 3000 m, the lower elevation limit for evaporites today.

In contrast, moving eastward into the eastern part of the Eastern Cordillera, Subandes, and Santa Bárbara Ranges, portions of almost the entire Cenozoic record are exposed but do not contain evaporites (DeCelles et al., 2011). Depending on stratigraphic level and location, these strata consist of a broad range of fluvial conglomerate, sandstone, and siltstone; paleosols; eolianites; and local lacustrine siltstone and marl. Evaporites are conspicuously absent, according to our surveys and many other studies (e.g., Starck and Vergani, 1996; Reynolds et al., 2000; Uba et al., 2006; Strecker et al., 2007; Carrapa et al., 2011a; DeCelles et al., 2011; Siks and Horton, 2011). Their absence is consistent with isotopic evidence for basin paleoelevations <3 km.

Volcanic Contributions to Surface Elevation

In general, the role of magmatic addition in the Cenozoic crustal thickening of the central Andes is thought to be minor compared to tectonic shortening, with volcanic rocks contributing as little as 1.5% of the crustal thickness today (Isacks, 1988; Haschke and Gunther, 2003). However insignificant this contribution is to the evolution of crustal thickness in the central Andes, the isostatically neutral redistribution of mass from the midcrust to the surface during eruptions would add to local surface elevations.

Arc volcanism and voluminous eruptions of Miocene–Quaternary silicic volcanic fields (such as the Altiplano-Puna volcanic complex, 10–1 Ma) contributed to surface elevation change in this sector of the central Andes. The Western Cordillera is an

Figure 9. Distribution of evaporites in geologic records from the central Andes, 22°S–26°S, showing the distribution (solid black dots) of evaporite ages. The arrow traces the approximate age and longitude of the eastward rise of the Andes to >3000 m in two steps (shaded in gray), first the Cordillera de Domeyko and most of the Puna by the late Eocene, followed by the Eastern Cordillera by the mid-Miocene.

andesite edifice upon which the modern active stratovolcanoes are built (e.g., Kay and Coira, 2009); the active volcanic centers rise 1–2 km above the average elevation of the Puna Plateau. In addition, ignimbrite lava flows can be tens to hundreds of meters thick and extend for tens of kilometers from source calderas, filling in topography and adding to surface elevations. Altiplano-Puna volcanic complex ignimbrite flows are distributed over an ~70,000 km² region of the central Andes (de Silva and Gosnold, 2007), although most flows are concentrated in areas around the volcanic centers and cover a total mapped area of ~17,000 km² (Francis and Hawkesworth, 1994). Using estimates of the productivity of andesitic arc volcanoes of the Central volcanic zone and previously compiled data on the age and estimated volumes of ignimbrite eruptions in the region (Francis and Hawkesworth, 1994; de Silva and Gosnold, 2007; Kay et al., 2010), we examined the timing and significance of the accumulation of volcanic material during the last 10 m.y.

The Cenozoic rate of andesitic volcanic addition in the Central volcanic zone is ~3 km³/m.y. per kilometer of arc length (Francis and Hawkesworth, 1994), and silicic supervolcanic eruptions periodically exceeded this rate. In this sector of the central Andes (22°S–26.5°S, ~500 km arc length), the andesitic arc has erupted ~1500 km³/m.y., and therefore ~18,000 km³ since 12 Ma (Fig. 10A). The silicic volcanic fields in the Central volcanic zone contributed significant additional material (Fig. 10A). The Altiplano-Puna volcanic complex extrusion rate exceeded the background rate of volcanism in the Central volcanic zone by at least an order of magnitude, with 200–2400 k.y. pulses of even higher rates of volcanism at ca. 10, 8, 6, and 4 Ma (de Silva and Gosnold, 2007). The total volume of material erupted during the Altiplano-Puna volcanic complex flare-up exceeded 10,000 km³ (Francis and Hawkesworth, 1994; de Silva and Gosnold, 2007). In the southern Puna (i.e., south of 24°S), Cerro Galán and other volcanic centers not considered part of the Altiplano-Puna volcanic complex erupted >1500 km³ (Kay et al., 2010) since the late Miocene (Fig. 10A).

To estimate the thickness of these accumulating volcanic rocks, we distribute the volumes over various conservatively large areas appropriate for the two voluminous types of arc volcanics: andesites and ignimbrites. Arc andesite volumes are distributed over swaths 100 km wide and as long as the arc length in question (Fig. 10B). Here, we make two Altiplano-Puna volcanic complex thickness estimates, one using an area of 17,000 km², and the other 35,000 km². Finally, the volumes of Puna ignimbrites from Kay et al. (2010) are distributed over areas estimated from maps provided by those authors. Note that the system is mass neutral and merely involves the redistribution of material from the lower or upper crust to the surface. Therefore, any change in density, say the change between a magma at kilometers depth to a frothy tuff at atmospheric pressure, will result in a volume change that is not compensated by isostasy.

The results of this simplified approach suggest that volcanic additions in the southern central Andes erupted >25,000 km³ of material since 12 Ma, which would result in 500–1000 m of sur-

face height gain across the entire region. The andesitic edifice in the Western Cordillera likely gained ~400 m of average surface height (Fig. 10B). Ignimbrites between 22°S–26.5°S contributed ~200–600 m of surface elevation in the last 10 m.y., with greater additions in the northern part of the study area that includes the Altiplano-Puna volcanic complex. At the center of the Altiplano-Puna volcanic complex activity, ignimbrites likely contributed
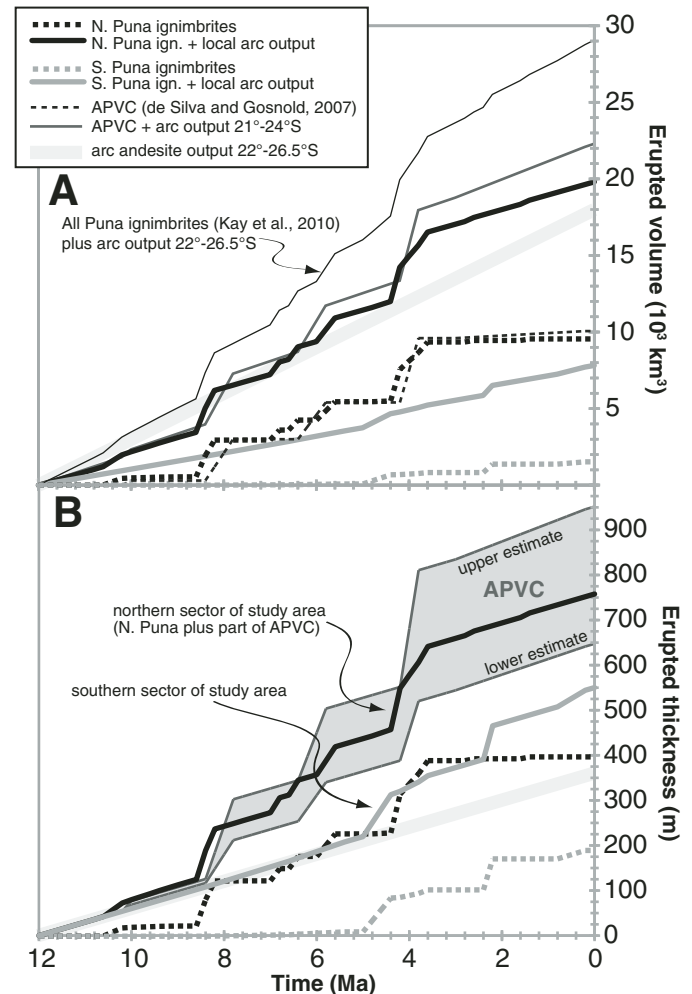

Figure 10. Estimates of the volume and thickness of volcanics erupted 21°S–26.5°S in the central Andes. Dotted lines indicate cumulative ignimbrite eruptions; solid lines combine ignimbrite results with the rate of andesite production, ~3 km³/m.y. per kilometer of arc length (Francis and Hawkesworth, 1994). (A) Cumulative erupted volumes of the Altiplano-Puna volcanic complex (APVC; 21°S–24°S; de Silva and Gosnold, 2007), Puna ignimbrites (22°S–26.5°S; northern Puna ignimbrites include some but not all of the Altiplano-Puna volcanic complex centers, notably excluding Pastos Grandes; Kay et al., 2010), and "background" andesite arc accumulation (22°S–26.5°S; Francis and Hawkesworth, 1994). (B) Cumulative volcanic thickness estimates for arc andesites and ignimbrites. Northern Puna ignimbrites were spread over 17,000 km² (the local andesites over 28,000 km²), and southern Puna ignimbrites were spread over 8000 km² (local andesites over 17,500 km²). Cumulative arc and ignimbrite curves (solid lines) from the same region are combined so they stack on each other.

~600–1000 m of surface elevation (Fig. 10B). These calculations are consistent with previous estimates, i.e., that the volcanics in the region compose the upper ~0.3–0.5 km of the Altiplano-Puna crust (Isacks, 1988), with locally thicker and thinner volcanics.

SYNTHETIC HISTORY AND BROADER IMPLICATIONS

The geologic and isotopic evidence converges on a coherent and detailed picture of the tectono-topographic evolution of the central Andes during the Cenozoic. The Andes grew upward and eastward in three main stages: The largest event occurred during the Eocene (the "Incaic orogeny" of older literature), when the western half the Andes attained >3–4 km elevation, followed by the gradual growth of the Eastern Cordillera in the Oligocene–Miocene, and the modern Subandes and Santa Bárbara Ranges after ca. 8 Ma (Fig. 11).

Late Cretaceous–Paleocene

The late Mesozoic to Paleocene magmatic arc was centered in what is now western Chile; a foredeep covered central Chile; and a rift system—the "Salta Rift"—occupied the back arc in westernmost Argentina (Fig. 11A; Salfity and Marquillas, 1994). East of the magmatic arc, most of what is now the Andes was covered by large lakes and coastal plains, represented by the Balbuena Subgroup, interspersed with residual paleotopographic highs of the Salta Rift and perhaps a more expansive Huaytiquina High (Mpodozis et al., 2005). The only paleoaltimetric or paleoclimatic information on the magmatic arc at this time is the presence of evaporites in the poorly dated (mid-Cretaceous?) Tonel Formation. Whatever its age, the presence of evaporites in the Tonel Formation demonstrates very dry conditions that require orographic blockage of rainfall to the east. However, we are hesitant to assign high elevations to the Tonel basin itself, in contrast to Cenozoic evaporites, because South America was not under strong compression during all of the Cretaceous. Since the opening of the South Atlantic during the Early Cretaceous, spreading rates have been variable (Torsvik et al., 2009), and slower rates may explain the Salta rift system during the Late Cretaceous.

Paleocene–Eocene

During the Eocene, the western part of the Andes—fully 50% of its modern cross section—rose to elevations of 3–4 km (Fig. 11B). This period of extensive Eocene deformation has
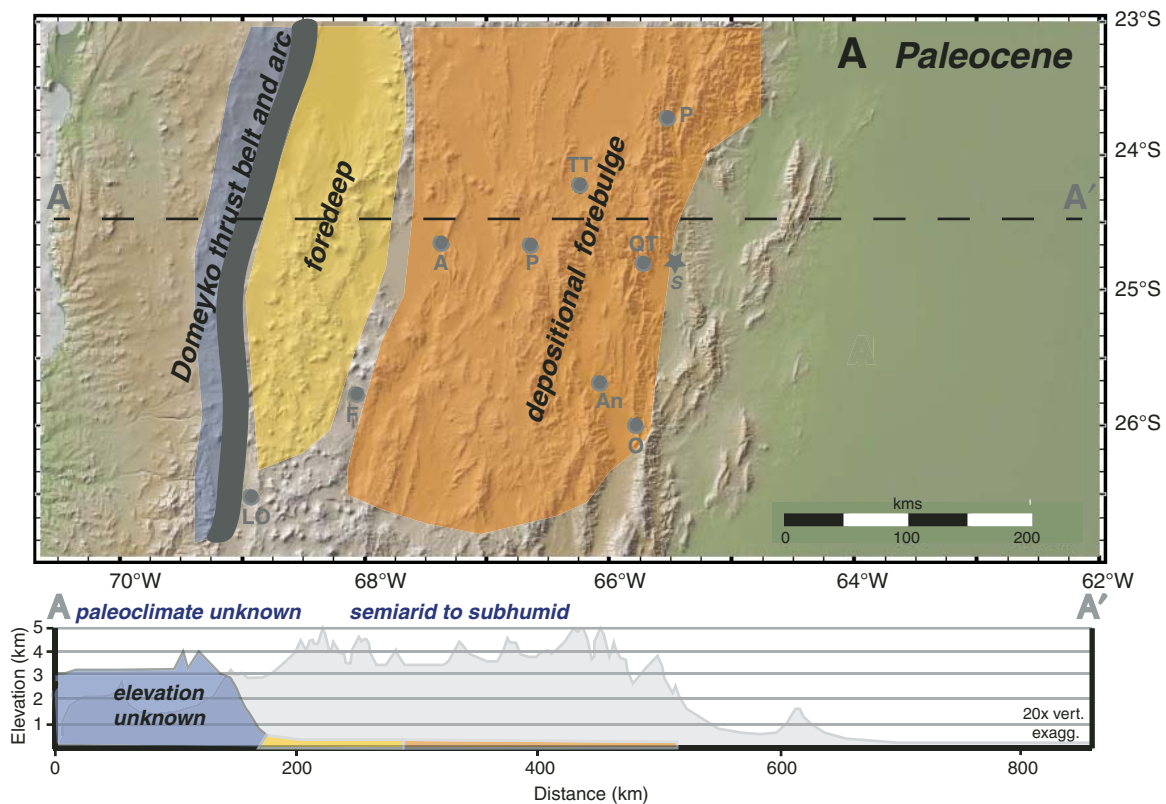
Figure 11 (*Continued on following pages*). Growth of the central Andes 23°S–27°S by the end of the (A) Paleocene, (B) late Eocene, (C) mid-Miocene, (D) late Miocene, (E) present, showing the approximate age intervals for accretion of each stage of the Andes from A to D. Topographic profile of the modern Andes is shown in background of cross sections. Letters are abbreviations of sampled sections shown on Figure 1. Thick gray line denotes the approximate position of the topographic/strain front.
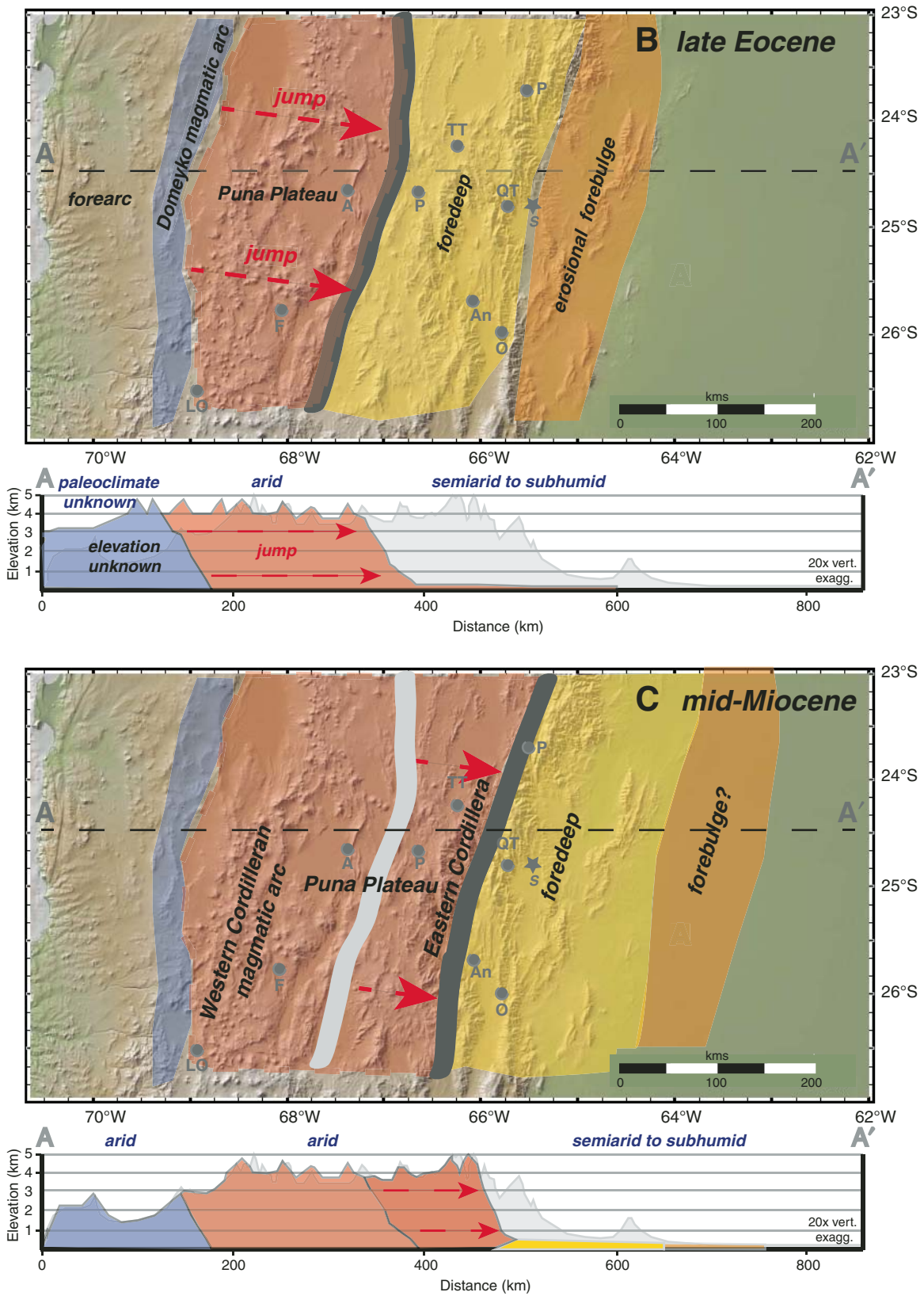
Quade et al.

Figure 11 (*Continued*).
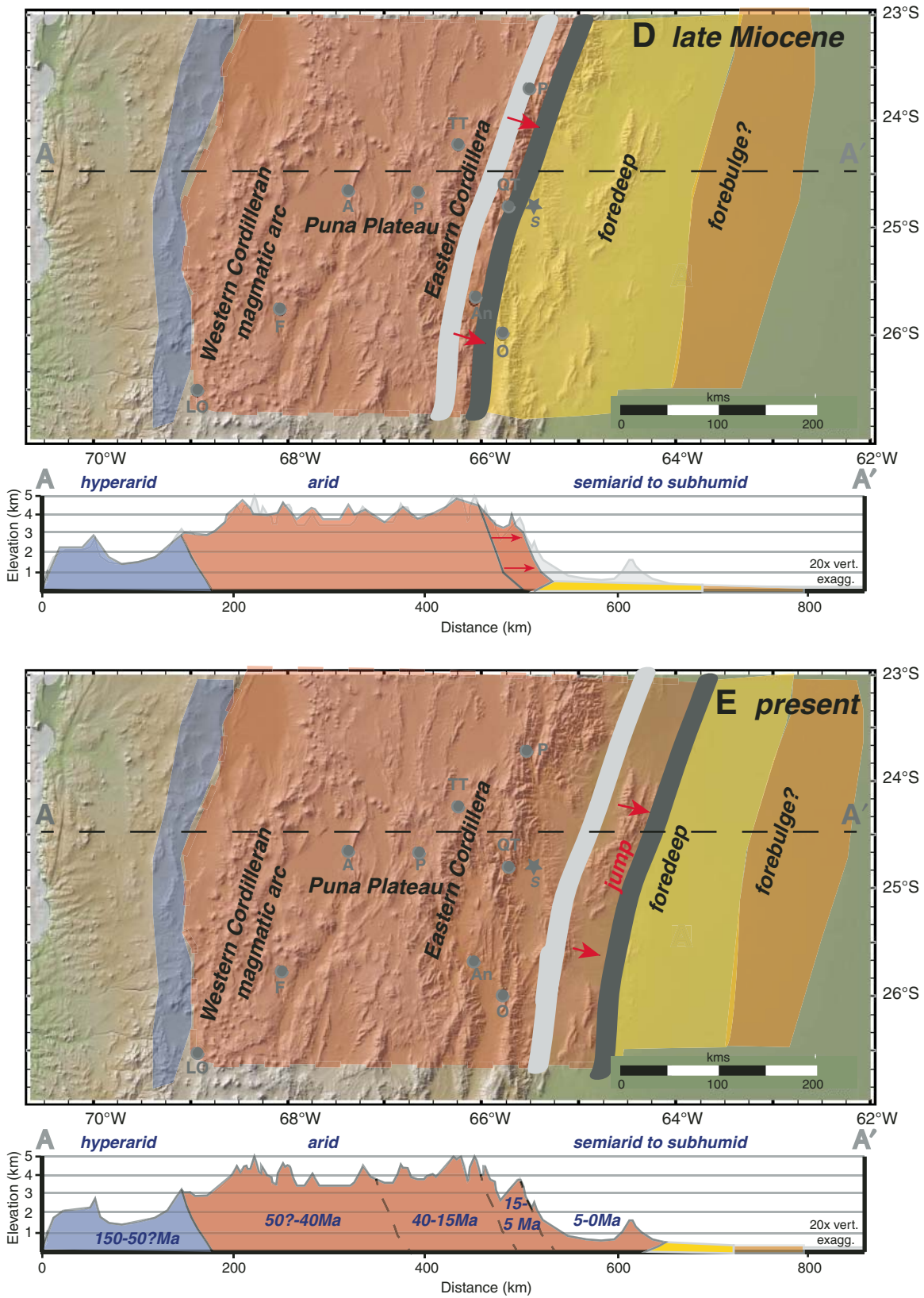
The growth of the central Andes, 22°S–26°S

Figure 11 (*Continued*).

long been recognized in the Andes of Peru, Bolivia, and Argentina (Steinmann, 1929; Mégard, 1984; Mpodozis et al., 2005). A regional-scale flexural foreland basin developed to the east of the orogen, and the corresponding flexural wave migrated eastward at a rate >20 mm/yr during the period 50–40 Ma between 22°S and 26°S (DeCelles et al., 2011). The magmatic arc was narrowly focused along 69°W–69.5°W in the Cordillera de Domeyko in central Chile, 50–150 km to the west of its present location (Fig. 11A; Trumbull et al., 2006). We have no paleoaltimetric information on these volcanoes. Immediately east of the magmatic arc, evaporites in the upper Naranja Formation (Paleocene?; Arriagiada et al., 2006) signify arid conditions, at a minimum pointing to the orographic blockage of the easterlies by high elevations farther to the east, and very probably indicating high (>3 km) paleoelevations at this time. This inference, combined with low δD values from glass starting by ca. 38 Ma from the Salar de Fraile and Arizaro Basin, suggests that the Cordillera de Domeyko and most of the Puna Plateau had attained an elevation of ~4 km by ca. 38 Ma. Extensive evaporites interbedded with these tuffs also point to high elevations and, combined with the lack of paleosols, bioturbation, and fossils, attest to arid conditions since the Paleogene at this latitude.

Eastward, intermontane deposits such as in the Salares de Fraile and Arizaro give way to clastic fluvial and alluvial-fan deposits of the Upper Eocene Geste Formation, now cropping out at 67°W just west of Salar de Pastos Grandes (Fig. 1). The Geste Formation has been interpreted as wedge-top deposits marking the position of the late Eocene orogenic strain front (DeCelles et al., 2007; Carrapa and DeCelles, 2008) and therefore the eastern topographic front of the Eocene Andes. Thermochronologic evidence from this time period shows that exhumation, especially 50–30 Ma, was extensive across the width of the orogen, from the Cordillera de Domeyko in the west (Maksaev and Zentilli, 1999) to mountain ranges delivering sediment to the Geste Formation on the east (Carrapa and DeCelles, 2008). Despite the extensive deformation, however, exhumation was shallow, << 7–8 km everywhere across the Incaic Andes, as indicated by (U-Th)/He and apatite fission-track data (Reiners et al., this volume; Carrapa et al., this volume).

East of this topographic break at ~67°W, basin filling in response to flexural subsidence commenced during the Paleocene–early Eocene, in the area now comprising the Eastern Cordillera. Carbonates in these basin deposits, represented by the Santa Bárbara and Metán Subgroups, show that this foreland basin setting was <1 km elevation through at least the end of the Oligocene, and was climatically semiarid to subhumid, as it is today. Low elevations are consistent with the forebulge and backbulge setting of the Paleocene–early Eocene deposits envisioned by DeCelles et al. (2011).

Oligocene to Late Miocene (ca. 35–5 Ma)

During the Oligocene–early Miocene, the eastern margins of the Puna Plateau and the Eastern Cordillera began to rise and propagate slowly eastward (Fig. 11C), coeval with subduction erosion (Stern, 1991) and aridification (Strecker et al., 2007). The slow eastward propagation of the orogenic strain front from ca. 35 Ma to ca. 5 Ma is tracked by a slowly migrating (~4 mm/yr) flexural wave in the coeval foreland basin system and by exhumation (DeCelles et al., 2011; Carrapa et al., 2011b). Intermontane basins in a probable upland setting continued to receive coarse clastic sediments, eolianites (during the early Miocene), evaporites, and tephras in the western and central portions of the Andes. The uplands expanded to the east as the topographic front of the Andes migrated slowly eastward ~150 km, hydrographically isolating and desiccating basins by the mid-Miocene as far east as 66.5°W. The orogenic front was in the Angastaco area at 66°W by ca. 14 Ma, deforming and exhuming older foredeep deposits and depositing syndeformational sandstones and conglomerates of the Angastaco Formation (Carrapa et al., 2011a, 2011b).

Evidence of gradual eastward stepping (Carrapa et al., 2011b; Carrapa and DeCelles, this volume; Reiners et al., this volume) of exhumation across the eastern Puna Plateau and into the Eastern Cordillera is documented by a number of thermochronologic studies: Sierra de Calalaste and Cobres Granite at 24–29 Ma (Carrapa et al., 2005; Deeken et al., 2006); the Cumbres de Luracatao, Complejo Oire, and others at 17–20 Ma (Deeken et al., 2006); and the Cachi Range by 15 Ma (Fig. 1; Coutand et al., 2006; Deeken et al., 2006; Carrapa et al., 2014a). To some extent, volcanism also followed these patterns, being characterized by (1) a magmatic gap during much of the Oligocene, (2) post-Oligocene eastward stepping of eruptive centers, with the Western Cordillera arc centered at ~68.5°W, and (3) a gradual eastward broadening of volcanism and proliferation of ignimbrites.

We have no stable isotopic evidence from individual continuous stratigraphic sections that might illustrate the progression of uplift of the eastern Puna Plateau and Eastern Cordillera from near sea level during the Eocene to 3–4 km today. The region changed from a lowland foreland basin during early Miocene time to high elevation by late Miocene time (Carrapa and DeCelles, this volume), but sedimentary basins capable of archiving this progressive rise in elevation are not preserved. This is likely a result of the fact that once the region had become incorporated into the orogenic wedge and risen above the elevation of the active wedge-top depozone, it entered an erosive regime in which long-term sediment accommodation was precluded by rapid erosion in the rising mountains. Not until the orogenic plateau had expanded to include what now lies in the eastern Puna was the region able to again accommodate sediment. Another way to conceptualize this is that while the region was climbing from low elevation to high (i.e., plateau) elevation, it was incapable of storing sediment over the long term due to oscillatory filling and excavating processes like those described by Hilley and Strecker (2005).

Deposition and long-term preservation of sediment in the eastern Puna Plateau and Eastern Cordillera resumed during the middle to late Miocene with the accumulation of evaporites and tuffs at high elevations. The δD values from the tuffs show that

the Eastern Cordillera was >3.5 km in elevation by 8 Ma (this study), and perhaps as early as 14 Ma (Carrapa et al., this volume), which is corroborated by the appearance of evaporites in the eastern Puna ca. 15 Ma (Vandervoort et al., 1995).

At the same time, to the east, a low-lying foreland region occupied what is now the Santa Bárbara tectonomorphic domain (DeCelles et al., 2011). Because the orogenic load was expanding eastward at a slow rate, the flexural wave migrated very slowly (~4 mm/yr) through the region (DeCelles et al., 2011). Our stable isotopic evidence from carbonates shows that this foreland basin lay at <1 km elevation.

Late Miocene to Present

The present form of the Andes began to take shape with a second rapid migration in the position of the orogenic strain front into the Subandes and Santa Bárbara Ranges, where nearly all major deformation was focused from latest Miocene onward (Figs. 11D–11E; e.g., Reynolds et al., 2000; Carrapa et al., 2011a; DeCelles et al., 2011; Metcalf and Kapp, this volume). Deposition in arid intermontane basins across the Puna Plateau continued through to the present. Deformation was minor in the late Neogene Puna Plateau, with extension locally replacing shortening (Schoenbohm and Strecker, 2009). Late Miocene to Pliocene volcanism, especially associated with voluminous ignimbrites of the so-called Altiplano-Puna volcanic complex flare-up (de Silva, 1989), raised the elevation of the Western Cordillera and Puna Plateau by an average of ~0.5 km.

The eastward migration of the orogenic strain front drove the foreland basin flexural wave rapidly (>45 mm/yr) through the region, stacking wedge-top deposits of the Palo Pintado Formation on top of foredeep facies in the Angastaco and Quebrada de los Colorados Formations, culminating with intermontane basin development during deposition of the San Felipe Formation (Carrapa et al., 2011a). Modest elevations of ~1.5 km appear to have developed during Palo Pintado deposition (9–5 Ma; Bywater-Reyes et al., 2010). The Santa Bárbara Ranges rose to their current maximum elevation of ~2 km mostly in the last 2 m.y. (Reynolds et al., 2000; Hain et al., 2011).

Causes and Broader Implications

Overall, our results break new ground in showing that the western half of the Andes rose to 3–4 km by the late Eocene. We agree with Evenstar et al. (2009) and Jordan et al. (2010) that the western slope of the Andes could have stood ~2 km above the adjacent forearc (now at ~1–1.5 km) by the early to mid-Miocene, and rose an additional ~1 km since then, partly due to ignimbrite additions. Our results also show that these high elevations were in place by the late Eocene and encompassed the Cordillera de Domeyko and most of the Puna Plateau. Much of the rest of the Andes out to the Eastern Cordillera was elevated ≥3 km by ca. 15 Ma, and the Subandes are the focus of most recent growth in the past 5 m.y.

This uplift history provides support for some existing models of central Andean uplift but contradicts others. For example, Lamb and Davis (2003) suggested that drying of the Atacama Desert due to global cooling in the Neogene caused uplift of the Andes. In this view, hyperaridification of the Atacama by the mid-Miocene (Rech et al., 2010) starved sediment supply to the adjacent Peru Trench, increasing shear stresses in the subduction zone. According to Lamb and Davis (2003), this led to accelerated uplift of the Andes in the last 10–15 m.y. Clearly, this explanation does not hold up if most of the Andes was elevated >3 km prior to 15 Ma, as we suggest here. Our evidence does not preclude the role of aridity in influencing tectonics, in that aridification of the Andes probably has promoted sediment storage and slowed erosion in the Andes, thus contributing to its height and eastward expansion (e.g., Sobel et al., 2003).

Others have suggested that the Andes, not at this latitude but further north in the Altiplano, rose en masse from ≤2 km to 4 km since 10 Ma (Ghosh et al., 2006a; Garzione et al., 2008). In our view, the isotopic evidence presented in these papers for late Miocene uplift is quite convincing. However, we would caution that the data reported are from the eastern Altiplano, and it is premature to speculate about young uplift for the entire Andean orogen. Additional paleoelevation data are needed to assess the uplift history of the western Altiplano and adjacent Western Cordillera.

In our opinion, the original idea that changes in convergence rates between South America and the Nazca plate control uplift of the Andes (Pardo-Casas and Molnar, 1987) still has significant explanatory power. Convergence rates have fluctuated between rapid (15 cm/yr) during 50–40 Ma and 20–10 Ma and slower (5–10 cm/yr) rates during 70–50, 40–20, and 10–0 Ma (Pardo-Casas and Molnar, 1987; Somoza, 1998). Peak convergence rates coincided in time with the rise of the Cordillera de Domeyko (at around 50–40 Ma) and Eastern Cordillera (by 15 Ma). If this idea is correct, the question remains open on how high convergence rates translate into uplift. Overall shortening has been estimated to be >100–150 km for the Cenozoic at this latitude and in Bolivia (for summary, see Kley and Monaldi, 1998), creating mass-balance problems and instabilities. The excess shallow crust not eroded away contributes to mountain building. Deeper crust and lithosphere can be removed or redistributed in a variety of ways beyond crustal thickening, including ablative removal (Pope and Willet, 1998), foundering of eclogitized mantle lithosphere (Kay and Gordillo, 1994; Ducea and Saleeby, 1998; Zandt et al., 2004; Garzione et al., 2006, 2008; Ducea et al., 2013), or ductile lower-crustal flow and underthrusting (Allmendinger and Gubbels, 1996; Barke and Lamb, 2006).

Haschke et al. (2006) made an intriguing attempt to unify the disposal of mantle lithosphere by delamination with plate convergence rates, igneous activity, slab breakoff, and ultimately uplift to explain cycles of Andean mountain building, much as DeCelles et al. (2009) proposed for western North America. Building on Kay and Kay (1991) and many others, they suggest that periods of rapid convergence lead to high-flux igneous events and attendant lithospheric thickening and densification (by

eclogitization) of the mantle lithosphere and/or descending ocean slab. The eclogitic lithosphere is dense and therefore unstable, and it founders, causing uplift of the overlying crust as the dense eclogitic keel recycles into the asthenosphere. The sequence of events envisioned by Haschke et al. (2006) requires rapid con-vergence followed by high-flux volcanic events, followed by lithospheric foundering and uplift. Haschke et al. (2006) sum-marized the geochemical, geophysical, and geologic evidence in support of two such cycles in the Cenozoic (Fig. 12). The first cycle spanned 70–40 Ma, and our data suggest it culminated
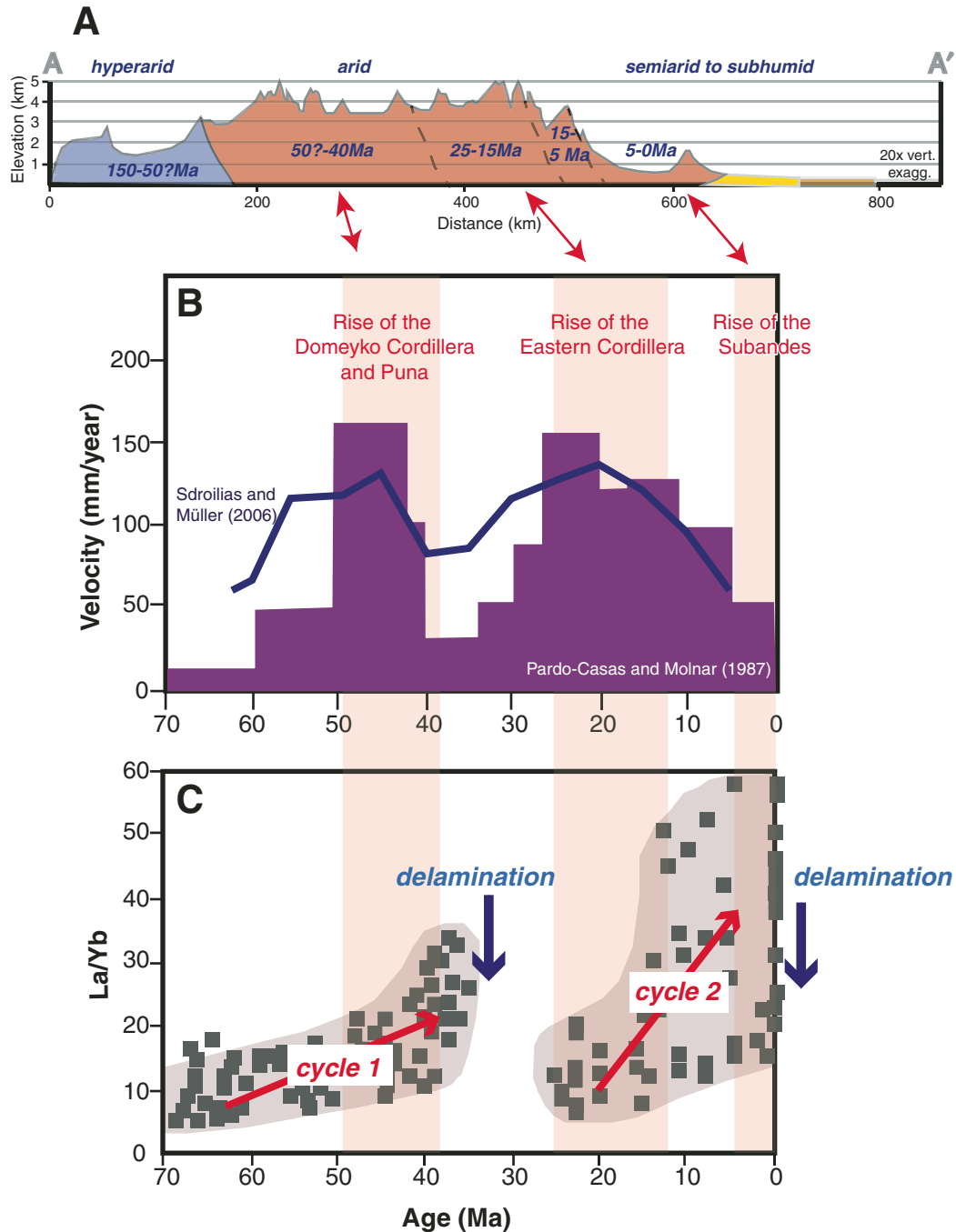
Figure 12. Summary of Andean uplift 22°S–26°S: (A) growth increments of the central Andes during the Cenozoic, (B) convergence rates between South America and the Nazca plate (modified from Pardo-Casas and Molnar, 1987; Somoza, 1998), and (C) cordilleran growth cycles as expressed by La/Yb ratios of Andean igneous rocks, modified from Haschke et al. (2006). La/Yb ratios are thought to positively correlate with crustal thickness. Blue arrows denote times of possible crustal foundering events.

in the rise of the western half of the Andes to high elevations by the late Eocene. The second cycle of increased convergence and volcanism occurred after the Oligocene magmatic gap starting ca. 25 Ma. This cycle plausibly culminated in the rise of the Eastern Cordillera by 15 Ma, completing construction of most of the modern Andes. Eruption of the voluminous Altiplano-Puna volcanic complex in the last 10 m.y. may be an expression of the ongoing status of this second "cordilleran" cycle (DeCelles et al., 2009), as the deformation front at this latitude stepped rapidly eastward, building the Subandes.

Despite these general correlations, the idea that lithospheric removal led to all Andean uplift does not appear consistent with our evidence. For one, according to isotopic evidence from Haschke et al. (2006), the first lithospheric removal event during the Cenozoic should have occurred early in the Oligocene ca. 35 Ma (Fig. 12). This would be too late to explain the Eocene uplift of the Cordillera de Domeyko and Puna Plateau. The 38 Ma date from tuffs and evaporites at base of the Fraile section provides the critical minimum age constraint for uplift to high elevation of the Puna Plateau. Therefore, we interpret the attainment of high elevations on the Puna Plateau by at least 38 Ma as a result of crustal thickening *preceding* lithospheric removal. Lastly, according to isotopic evidence from Haschke et al. (2006), the Andes is currently undergoing a second Cenozoic cycle of crustal thickening (not lithospheric removal), consistent with the second rapid phase of flexural wave propagation and the recent growth of the Subandes (Fig. 12; DeCelles et al., 2011).

New geochemical and geophysical evidence suggests that lithospheric removal has and currently is occurring beneath the Andes, but not on the sort of regional scale required to explain the three broad uplift events that we now recognize (Beck et al., this volume; Murray et al., this volume). Rather, geophysical data point to small-scale (<100 km^2), low-velocity zones, especially beneath recent large ignimbrite fields (Beck et al., this volume). If representative of the entire central Andes, our conclusions pose a challenge to our colleagues working to the north in the Altiplano, where studies suggest that lithospheric removal (Ghosh et al., 2006a; Garzione et al., 2006, 2008) is the cause of major uplift in that region. The Andes of Bolivia and southern Peru experienced similar convergence rates in the Cenozoic as our study area. The validity of our suggestion that crustal thickening, not lithospheric removal, plays a central role in uplift can be tested by an integrated, full-orogen reconstruction of uplift at that latitude. Special attention should be paid to the relatively unstudied western Andes, where we now know that uplift in the Puna was much earlier (Eocene) than previously recognized.

ACKNOWLEDGMENTS

REFERENCES CITED

Allmendinger, R., and Gubbels, T., 1996, Pure and simple shear plateau uplift—Puna, Argentina and Bolivia: Tectonophysics, v. 259, p. 1–13, doi:10.1016/0040-1951(96)00024-8.

Alonso, R.N., Jordan, T.E., Tabutt, K.T., and Vandervoort, D.S., 1991, Giant evaporite beds of the Neogene central Andes: Geology, v. 19, p. 401–404, doi:10.1130/0091-7613(1991)019<0401:GEBOTN>2.3.CO;2.

Arriagiada, C., Cobbold, P., and Roperch, P., 2006, Salar de Atacama Basin; a record of compressional tectonics in the central Andes since the mid-Cretaceous: Tectonics, v. 25, TC1008, doi:10.1029/2004TC001770.

Barke, R., and Lamb, S., 2006, Late Cenozoic uplift of the Eastern Cordillera, Bolivia: Earth and Planetary Science Letters, v. 249, p. 350–367, doi:10.1016/j.epsl.2006.07.012.

Barnes, J.B., Ehlers, T.A., Insel, N., McQuarrie, N., and Poulsen, C.J., 2012, Linking orography, climate, and exhumation across the central Andes: Geology, v. 40, no. 12, p. 1135–1138, doi:10.1130/G33229.1.

Beck, S.L., Zandt, G., Ward, K.M., and Scire, A., 2015, this volume, Multiple styles and scales of lithospheric foundering beneath the Puna Plateau, central Andes, *in* DeCelles, P.G., Ducea, M.N., Carrapa, B., and Kapp, P.A., eds., Geodynamics of a Cordilleran Orogenic System: The Central Andes of Argentina and Northern Chile: Geological Society of America Memoir 212, doi:10.1130/2015.1212(03).

Boyd, J., 2010, Tectonic Evolution of the Arizaro Basin of the Puna Plateau, NW Argentina: Implications for Plateau-Scale Processes [M.S. thesis]: Laramie, Wyoming, University of Wyoming, 83 p.

Bywater-Reyes, S., Carrapa, B., Clementz, M., and Schoenbohm, L., 2010, Effect of late Cenozoic aridification on sedimentation in the Eastern Cordillera of northwest Argentina (Angastaco Basin): Geology, v. 38, no. 3, p. 235–238, doi:10.1130/G30532.1.

Canavan, R.R., Carrapa, B., Clementz, M.T., Quade, J., DeCelles, P., and Schoenbohm, L.M., 2014, Early Cenozoic uplift of the Puna Plateau, central Andes, based on stable isotope paleoaltimetry of hydrated volcanic glass: Geology, v. 42, no. 5, p. 447–450, doi: 10.1130/G35239.1

Carrapa, B., and DeCelles, P.G., 2008, Eocene exhumation and basin development in the Puna of northwestern Argentina: Tectonics, v. 27, TC1015, doi: 10.1029/2007TC002127.

Carrapa, B., and DeCelles, P.G., 2015, this volume, Regional exhumation and kinematic history of the central Andes in response to cyclical orogenic processes, *in* DeCelles, P.G., Ducea, M.N., Carrapa, B., and Kapp, P.A., eds., Geodynamics of a Cordilleran Orogenic System: The Central Andes of Argentina and Northern Chile: Geological Society of America Memoir 212, doi:10.1130/2015.1212(11).

Carrapa, B., Adelmann, D., Hilley, G.E., Mortimer, E., Sobel, E.R., and Strecker, M.R., 2005, Oligocene range uplift and development of plateau morphology in the southern central Andes: Tectonics, v. 24, TC4011, doi:10.1029/2004TC001762.

Carrapa, B., Bywater-Reyes, S., DeCelles, P.G., Mortimer, E., and Gehrels, G.E., 2011a, Late-Pliocene basin evolution in the Eastern Cordillera of northwestern Argentina (25–26°S): Regional implications for Andean orogenic wedge development: Basin Research, v. 23, p. 1–20.

Carrapa, B., Trimble, J.D., and Stockli, D.F., 2011b, Patterns and timing of exhumation and deformation in the Eastern Cordillera of NW Argentina revealed by (U-Th)/He thermochronology: Tectonics, v. 30, TC3003, doi:10.1029/2010TC002707.

Carrapa, B., Bywater-Reyes, S., Safipour, R., Sobel, E.R., Schoenbohm, L.M., DeCelles, P.G., Reiners, P.W., and Stockli, D., 2014a, The effect of inherited paleotopography on exhumation of the Central Andes of NW Argentina: Geological Society of America Bulletin, v. 126, no. 1–2, p. 66–77, doi:10.1130/B30844.1.

Carrapa, B., Huntington, K.H., Clementz, M., Bywater-Reyes, S., Quade, J., Schoenbohm, L., and Canavan, R., 2014b, Uplift of the Central Andes of NW Argentina associated with upper crustal shortening,

revealed by multi-proxy isotopic analyses: Tectonics, p. 1039–1054, doi:10.1002/2013TC003461.

Cassel, E.J., Graham, S.A., and Chamberlain, C.P., 2009, Cenozoic tectonic and topographic evolution of the northern Sierra Nevada, California, through stable isotope paleoaltimetry of volcanic glass: Geology, v. 37, no. 6, p. 547–550, doi:10.1130/G25572A.1.

Cerling, T.E., and Quade, J., 1993, Stable carbon and oxygen isotopes in soil carbonates, *in* Swart, P., McKenzie, J.A., and Lohman, K.C., eds., Continental Indicators of Climate, Proceedings of Chapman Conference, Jackson Hole, Wyoming: American Geophysical Union Geophysical Monograph 78, p. 217–231.

Cohen, A., McGlue, M.M., Ellis, G.S., Zani, H., Swarzenski, P.W., Assine, M.L., and Silva, A., 2015, this volume, Lake formation, characteristics, and evolution in retroarc deposystems: A synthesis of the modern Andean orogen and its associated basins, *in* DeCelles, P.G., Ducea, M.N., Carrapa, B., and Kapp, P.A., eds., Geodynamics of a Cordilleran Orogenic System: The Central Andes of Argentina and Northern Chile: Geological Society of America Memoir 212, doi:10.1130/2015.1212(16).

Coutand, I., Carrapa, B., Deekin, A., Schmidt, A.K., Sobel, E.R., and Strecker, M.R., 2006, Propagation of orographic barriers along an active range front: Insights from sandstone petrography and detrital apatite fission-track thermochronology in the intramontane Angastaco Basin, NW Argentina: Basin Research, v. 18, p. 1–26, doi:10.1111/j.1365-2117.2006.00283.x.

DeCelles, P.G., Carrapa, B., and Gehrels, G.E., 2007, Detrital zircon U-Pb ages provide provenance and chronostratigraphic information from Eocene synorogenic deposits in northwestern Argentina: Geology, v. 35, no. 4, p. 323–326, doi:10.1130/G23322A.1.

DeCelles, P.G., Ducea, M.N., Kapp, P., and Zandt, G., 2009, Cyclicity in Cordilleran orogenic systems: Nature Geoscience, v. 2, p. 251–257, doi:10.1038/ngeo469.

DeCelles, P.G., Carrapa, B., Horton, B.K., and Gehrels, G.E., 2011, Cenozoic foreland basin system in the central Andes of northwestern Argentina: Implications for Andean geodynamics and modes of deformation: Tectonics, v. 30, TC6013, doi:10.1029/2011TC002948.

DeCelles, P.G., Zandt, G., Beck, S.L., Currie, C.A., Ducea, M.N., Kapp, P., Gehrels, G.E., Carrapa, B., Quade, J., and Schoenbohm, L.M., 2015, this volume, Cyclical orogenic processes in the Cenozoic central Andes, *in* DeCelles, P.G., Ducea, M.N., Carrapa, B., and Kapp, P.A., eds., Geodynamics of a Cordilleran Orogenic System: The Central Andes of Argentina and Northern Chile: Geological Society of America Memoir 212, doi:10.1130/2015.1212(22)

Deeken, A., Sobel, E.R., Coutano, I., Haschke, M., Riller, U., and Strecker, M.R., 2006, Development of the southern Eastern Cordillera, NW Argentina, constrained by apatite fission track thermochronology: From Early Cretaceous extension to middle Miocene shortening: Tectonics, v. 25, TC6003, doi:10.1029/2005TC001894.

Dennis, K.J., and Schrag, D.P., 2010, Clumped isotope thermometry of carbonitites as an indicator of diagenetic alteration: Geochimica et Cosmochimica Acta, v. 74, p. 4110–4122, doi:10.1016/j.gca.2010.04.005.

Dennis, K.J., Affek, H.P., Passey, B.H., Schrag, D.P., and Eiler, J.M., 2011, Defining the absolute reference frame for clumped isotope studies of CO_2: Geochimica et Cosmochimica Acta, v. 75, p. 7117–7131, doi:10.1016/j.gca.2011.09.025.

de Silva, S., 1989, Altiplano-Puna volcanic complex of the central Andes: Geology, v. 17, no. 12, p. 1102–1106, doi:10.1130/0091-7613 (1989)017<1102:APVCOT>2.3.CO;2.

de Silva, S.L., and Gosnold, W.D., 2007, Episodic construction of batholiths: Insights from the spatiotemporal development of an ignimbrite flare-up: Journal of Volcanology and Geothermal Research, v. 167, no. 1–4, p. 320–335, doi:10.1016/j.jvolgeores.2007.07.015.

Dettinger, M.P., and Quade, J., 2015, this volume, Testing the analytical protocols and calibration of volcanic glass for the reconstruction of hydrogen isotopes in paleoprecipitation, *in* DeCelles, P.G., Ducea, M.N., Carrapa, B., and Kapp, P.A., eds., Geodynamics of a Cordilleran Orogenic System: The Central Andes of Argentina and Northern Chile: Geological Society of America Memoir 212, doi:10.1130/2015.1212(14).

Ducea, M., and Saleeby, J., 1998, The age and origin of a thick-ultramafic keel from beneath the Sierra Nevada batholith: Contributions to Mineralogy and Petrology, v. 133, p. 169–185, doi:10.1007/s004100050445.

Ducea, M.N., Seclaman, A.C., Murray, K.E., Jianu, D., and Schoenbohm, L.M., 2013, Mantle-drip magmatism beneath the Altiplano-Puna Plateau, central Andes: Geology, v. 41, no. 8, p. 915–918, doi:10.1130/G34509.1.

Echavarria, L., Hernandez, R., Allmendinger, R., and Reynolds, J., 2003, Subandean thrust and fold belt of northwestern Argentina; geometry and timing of Andean evolution: American Association of Petroleum Geologists Bulletin, v. 87, no. 6, p. 965–985, doi:10.1306/01200300196.

Ehlers, T.A., and Poulsen, C.J., 2009, Influence of Andean uplift on climate and paleoaltimetry estimates: Earth and Planetary Science Letters, v. 281, p. 238–248, doi:10.1016/j.epsl.2009.02.026.

Eiler, J.M., and Schauble, E.A., 2004, $^{18}O^{13}C^{16}O$ in Earth's atmosphere: Geochimica et Cosmochimica Acta, v. 68, no. 23, p. 4767–4777, doi:10.1016/j.gca.2004.05.035.

Evenstar, L.A., Hartley, A.J., Stuart, F.M., Mather, A.E., Rice, C.M., and Chong, G., 2009, Multiphase development of the Atacama planation surface recorded by cosmogenic ^{3}He exposure ages: Implications for uplift and Cenozoic climate change in western South America: Geology, v. 37, no. 1, p. 27–30, doi:10.1130/G25437A.1.

Francis, P., and Hawkesworth, C., 1994, Late Cenozoic rates of magmatic activity in the central Andes and their relationships to continental-crust formation and thickening: Journal of the Geological Society, London, v. 151, p. 845–854, doi:10.1144/gsjgs.151.5.0845.

Friedman, I., Gleason, J., Sheppard, R.A., and Gude, A.J., 1993, Deuterium fractionation as water diffuses into silicic volcanic ash, *in* Swart, P., McKenzie, J.A., and Lohman, K.C., eds., Continental Indicators of Climate, Proceedings of Chapman Conference, Jackson Hole, Wyoming: American Geophysical Union Geophysical Monograph 78, p. 321–323.

Garzione, C., Molnar, P., Libarkin, J.C., and MacFadden, B.J., 2006, Rapid late Miocene rise of the Bolivian Altiplano: Evidence for removal of the mantle lithosphere: Earth and Planetary Science Letters, v. 241, p. 543–556, doi:10.1016/j.epsl.2005.11.026.

Garzione, C., Hoke, G., Libarkin, J., and Withers, S., 2008, Rise of the Andes: Science, v. 320, p. 1304–1307, doi:10.1126/science.1148615.

Gehrels, G.E., Valencia, V., and Ruiz, J., 2008, Enhanced precision, accuracy, efficiency, and spatial resolution of U-Pb ages by laser ablation–multicollector–inductively coupled plasma–mass spectrometry: Geochemistry Geophysics Geosystems, v. 9, Q03017, doi:10.1029/2007GC001805.

Ghosh, P., Eiler, J.M., and Garzione, C., 2006a, Rapid uplift of the Altiplano revealed in abundances of ^{13}C–^{18}O bonds in paleosol carbonate: Science, v. 311, p. 511–515, doi:10.1126/science.1119365.

Ghosh, P., Adkins, J., Affek, H., Balta, B., Guo, W., Schauble, E.A., Schrag, D., and Eiler, J.M., 2006b, ^{13}C–^{18}O bonds in carbonate minerals: A new kind of paleothermometer: Geochimica et Cosmochimica Acta, v. 70, p. 1439–1456, doi:10.1016/j.gca.2005.11.014.

Gregory-Wodzicki, K.M., 2000, Uplift history of the central northern Andes: Geological Society of America Bulletin, v. 112, no. 7, p. 1091–1105, doi:10.1130/0016-7606(2000)112<1091:UHOTCA>2.0.CO;2.

Hain, M.P., Stecjer, M.R., Bookhagen, B., Alonso, R.N., Pingel, H., and Schmitt, A.K., 2011, Neogene to Quaternary broken foreland formation and sedimentation dynamics in the Andes of NW Argentina (25°S): Tectonics, v. 30, TC2006, doi:10.1029/2010TC002703.

Hartley, A.J., Flint, S., Tuner, P., and Jolley, E.J., 1992, Tectonic controls on the development of a semi-arid, alluvial basin as reflected in the stratigraphy of the Purilactis Group (Upper Cretaceous–Eocene), northern Chile: Journal of South American Earth Sciences, v. 5, p. 275–296, doi:10.1016/0895-9811(92)90026-U.

Haschke, M., and Gunther, A., 2003, Balancing crustal thickening in arcs by tectonic vs. magmatic means: Geology, v. 31, no. 11, p. 933–936, doi:10.1130/G19945.1.

Haschke, M., Gunther, A., Melnick, D., Echtler, H., Reutter, K.J., Scheuber, E., and Oncken, O., 2006, Central and southern Andean tectonic evolution inferred from arc magmatism, *in* Oncken, O., Chong, G., Franz, G., Giese, P., Götze, H., Ramos, V.A., Strecker, M.R., and Wigger, P., eds., The Andes—Active Subduction Orogeny: Berlin, Springer-Verlag, Frontiers in Earth Sciences, v. 1, p. 337–353.

Henkes, G.A., Passey, B.H., Grossman, E.L., Shenton, B.J., Pérez-Huerta, A., and Yancey, T.E., 2014, Temperature limits for preservation of primary calcite clumped isotope paleotemperatures: Geochimica et Cosmochimica Acta, v. 139, p. 362–382, doi:10.1016/j.gca.2014.04.040.

Hilley, G.E., and Strecker, M.R., 2005, Processes of oscillatory basin filling and excavation in a tectonically active orogen: Quebrada del Toro Basin, NW Argentina: Geology, v. 117, no. 7–8, p. 887–901.

Hoke, G.D., and Garzione, C.N., 2008, Paleosurfaces, paleoelevation, and the mechanisms for the late Miocene topographic development of the

The growth of the central Andes, 22°S–26°S

Altiplano Plateau: Earth and Planetary Science Letters, v. 271, p. 192–201, doi:10.1016/j.epsl.2008.04.008.

Hongn, F.D., del Papa, C., Powell, J., Petrinovic, I., Mon, R., and Deraco, V., 2007, Middle Eocene deformation and sedimentation in the Puna–Eastern Cordillera transition (23′26°S); control of pre-existing heterogeneities on the pattern of initial Andean shortening: Geology, v. 35, p. 271–274, doi:10.1130/G23189A.1.

Horton, B., 1999, Erosional control on the geometry and kinematics of thrust belt development in the central Andes: Tectonics, v. 18, no. 6, p. 1292–1304, doi:10.1029/1999TC900051.

Humphrey, N.F., and Konrad, S.K., 2000, River incision or diversion in response to bedrock uplift: Geology, v. 28, p. 43–46, doi:10.1130/0091-7613(2000)28<43:RIODIR>2.0.CO;2.

Huntington, K.W., Eiler, J.M., Affek, H.P., Guo, W., Bonifacie, M., Yeung, L.Y., Thiagarajan, N., Passey, B., Tripati, A., Daëron, M., and Came, R., 2009, Methods and limitations of "clumped" CO_2 isotope (Δ_{47}) analysis by gas-source isotope ratio mass spectrometry: Journal of Mass Spectrometry, v. 44, p. 1318–1329, doi:10.1002/jms.1614.

Huntington, K.W., Saylor, J., Quade, J., and Hudson, A.M., 2014, High Late Miocene-Pliocene elevation of the Zhada basin, SW Tibetan plateau, from clumped isotope thermometry: Geological Society of America Bulletin, doi:10.1130/B31000.1.

Isacks, B., 1988, Uplift of the central Andean Plateau and bending of the Bolivian orocline: Journal of Geophysical Research–Solid Earth and Planets, v. 93, no. B4, p. 3211–3231.

Jordan, T.E., Nester, P.L., Blanco, N., Hoke, G.D., Dávila, F., and Tomlinson, A.J., 2010, Uplift of the Altiplano-Puna Plateau: A view from the west: Tectonics, v. 29, TC5007, doi:10.1029/2010TC002661.

Kay, R.W., and Kay, S.M., 1991, Creation and destruction of lower continental crust: Geologische Rundschau, v. 80, p. 259–278, doi:10.1007/BF01829365.

Kay, S.M., and Gordillo, C.E., 1994, Pocho volcanic rocks and the melting of depleted continental lithosphere above a shallowly dipping subduction zone in the central Andes: Contributions to Mineralogy and Petrology, v. 117, p. 25–44, doi:10.1007/BF00307727.

Kay, S.M., and Coira, B., 2009, Shallowing and steepening subduction zones, continental lithospheric loss, magmatism, and crustal flow under the central Andes, *in* Kay, S.M., Ramos, V.A., and Dickinson, W.R., eds., Backbone of the Americas: Shallow Subduction, Plateau Uplift, and Ridge and Terrane Collision: Geological Society of America Memoir 204, p. 229–259.

Kay, S.M., Coira, B.L., Caffe, P.J., and Chen, C.-H., 2010, Regional chemical diversity, crustal and mantle sources and evolution of central Andean Puna Plateau ignimbrites: Journal of Volcanology and Geothermal Research, v. 198, no. 1–2, p. 81–111, doi:10.1016/j.jvolgeores.2010.08.013.

Kim, S.-T., and O'Neil, J.R., 1997, Equilibrium and nonequilibrium oxygen isotope effects in synthetic carbonates: Geochimica et Cosmochimica Acta, v. 61, no. 16, p. 3461–3475, doi:10.1016/S0016-7037(97)00169-5.

Kley, J., and Monaldi, C.R., 1998, Tectonic shortening and crustal thickness in the central Andes: How good is the correlation: Geology, v. 26, no. 8, p. 723–726, doi:10.1130/0091-7613(1998)026<0723:TSACTI>2.3.CO;2.

Kraemer, B., Adelmann, D., Alten, M., Schurr, W., Erpenstein, K., Kiefer, E., van den Bogaard, P., and Görler, K., 1999, Incorporation of the Paleogene foreland into the Neogene Puna Plateau: The Salar de Antofalla area, NW Argentina: Journal of South American Earth Sciences, v. 12, p. 157–182, doi:10.1016/S0895-9811(99)00012-7.

Lamb, S., and Davis, S.D., 2003, Cenozoic climate change as a possible cause for the rise of the Andes: Nature, v. 425, p. 792–797, doi:10.1038/nature02049.

Maksaev, V., and Zentilli, M., 1999, Fission track thermochronology of the Domeyko Cordillera, northern Chile; implications for Andean tectonics and porphyry copper metallogenesis: Exploration and Mining Geology, v. 8, no. 1–2, p. 65–89.

Marquillas, R., Sabino, I., Sial, A.N., del Papa, C., Ferreira, V., and Mathews, S., 2007, Carbon and oxygen isotopes of Maastrichtian–Danian shallow marine carbonates: Yacoraite Formation, northwestern Argentina: Journal of South American Earth Sciences, v. 23, p. 304–320, doi:10.1016/j.jsames.2007.02.009.

Mégard, F., 1984, The Andean orogenic period and its major structures in central and northern Peru: Journal of the Geological Society, London, v. 141, p. 893–900, doi:10.1144/gsjgs.141.5.0893.

Metcalf, K., and Kapp, P., 2015, this volume, Along-strike variations in crustal seismicity and modern lithospheric structure of the central Andean

forearc, *in* DeCelles, P.G., Ducea, M.N., Carrapa, B., and Kapp, P.A., eds., Geodynamics of a Cordilleran Orogenic System: The Central Andes of Argentina and Northern Chile: Geological Society of America Memoir 212, doi:10.1130/2015.1212(04).

Mpodozis, C., Arriagiada, C., Basso, M., Roperch, P., Cobbold, P., and Reich, M., 2005, Late Mesozoic to Paleogene stratigraphy of the Salar de Atacama Basin, Antofagasta, northern Chile: Implications for the tectonic evolution of the central Andes: Tectonophysics, v. 399, p. 125–154, doi:10.1016/j.tecto.2004.12.019.

Mulch, A., Sarna-Wojdicki, A.M., Perkins, M.E., and Chamberlain, C.P., 2008, A Miocene to Pleistocene climate and elevation record of the Sierra Nevada (California): Proceedings of the National Academy of Sciences of the United States of America, v. 105, no. 19, p. 6819–6824, doi:10.1073/pnas.0708811105.

Murray, K.E., Ducea, M.N., and Schoenbohm, L., 2015, this volume, Foundering-driven lithospheric melting: The source of central Andean mafic lavas on the Puna Plateau (22°S–27°S), *in* DeCelles, P.G., Ducea, M.N., Carrapa, B., and Kapp, P.A., eds., Geodynamics of a Cordilleran Orogenic System: The Central Andes of Argentina and Northern Chile: Geological Society of America Memoir 212, doi:10.1130/2015.1212(08).

Palma, R.M., 2000, Lacustrine facies in the upper Cretaceous Balbuena subgroup (Salta Group): Andina Basin, Argentina, *in* Gierolowski-Kordesch, E.H., and Kelts, K.R., eds., Lake Basins through Space and Time: American Association of Petroleum Geologists, Studies in Geology, v. 46, p. 323–328.

Pardo-Casas, F., and Molnar, P., 1987, Relative motion of the Nazca (Farallon) plate since Late Cretaceous time: Tectonics, v. 6, no. 3, p. 233–248, doi:10.1029/TC006i003p00233.

Passey, B.H., and Henkes, G.A., 2012, Carbonate clumped isotope bond reordering and geospeedometry: Earth and Planetary Science Letters, v. 351–352, p. 223–236, doi:10.1016/j.epsl.2012.07.021.

Passey, B.H., Levin, N.E., Cerling, T.E., Brown, F.H., and Eiler, J.M., 2010, High-temperature environments of human evolution in East Africa based on bond-ordering in paleosol carbonates: Proceedings of the National Academy of Sciences of the United States of America, v. 107, no. 25, p. 11,245–11,249, doi:10.1073/pnas.1001824107.

Pope, D.C., and Willet, S.D., 1998, Thermal-mechanical model for crustal thickening in the central Andes driven by ablative subduction: Geology, v. 26, p. 511–514, doi:10.1130/0091-7613(1998)026<0511:TMMFCT>2.3.CO;2.

Quade, J., Rech, J., Latorre, C., Betancourt, J., Gleason, E., and Kalin-Arroyo, M., 2007, Soils at the hyperarid margin: The isotopic composition of soil carbonate from the Atacama Desert: Geochimica et Cosmochimica Acta, v. 71, p. 3772–3795, doi:10.1016/j.gca.2007.02.016.

Quade, J., Eiler, J., Daëron, M., and Achuythan, H., 2013, The clumped isotope paleothermometer in soils and paleosol carbonate: Geochimica et Cosmochimica Acta, v. 105, p. 92–107, doi:10.1016/j.gca.2012.11.031.

Rech, J.A., Currie, B.S., Shullenberger, E.D., Dunagan, S.P., Jordan, T.E., Blanco, N., Tomlinson, A.J., Rowe, H.D., and Houston, J., 2010, Evidence for the development of the Andean rain shadow from a Neogene isotopic record in the Atacama Desert, Chile: Earth and Planetary Science Letters, v. 292, p. 371–382, doi:10.1016/j.epsl.2010.02.004.

Reiners, P.W., Thomson, S.N., Vernon, A., Willett, S.D., Zattin, M., Einhorn, J., Gehrels, G., Quade, J., Pearson, D., Murray, K.E., and Cavazza, W., 2015, this volume, Low-temperature thermochronologic trends across the central Andes, 21°S–28°S, *in* DeCelles, P.G., Ducea, M.N., Carrapa, B., and Kapp, P.A., eds., Geodynamics of a Cordilleran Orogenic System: The Central Andes of Argentina and Northern Chile: Geological Society of America Memoir 212, doi:10.1130/2015.1212(12).

Reynolds, J., Galli, C., Hernández, R., Idleman, B., Kotila, J., Hilliard, R., and Naeser, C., 2000, Middle Miocene tectonic development of the Transition zone, Salta Province, northwest Argentina: Magnetic stratigraphy from the Metán Subgroup, Sierra de González: Geological Society of America Bulletin, v. 112, p. 1736–1751, doi:10.1130/0016-7606(2000)112<1736:MMTDOT>2.0.CO;2.

Rowley, D.B., and Garzione, C.N., 2007, Stable isotope-based paleoaltimetry: Annual Review of Earth and Planetary Sciences, v. 35, p. 463–508, doi:10.1146/annurev.earth.35.031306.140155.

Salfity, J.A., and Marquillas, R.A., 1994, Tectonics and sedimentary evolution of the Cretaceous–Eocene Salta Group Basin, Argentina, *in* Salfity, J.A., ed., Cretaceous Tectonics of the Andes: Braunschweig-Wiesbaden, Germany, Friedrich Viewig and Sohn, Earth Evolution Sciences, p. 266–315.

Schoenbohm, L.M., and Carrapa, B., 2011, Evidence from timing of contraction, extension, sedimentation, and magmatism for small-scale lithospheric foundering in the Puna Plateau, NW Argentina: San Francisco, California, American Geophysical Union, Fall meeting, abstract T13I-07.

Schoenbohm, L.M., and Strecker, M.R., 2009, Normal faulting along the southern margin of the Puna Plateau, northwest Argentina: Tectonics, v. 28, no. 5, TC5008, doi:10.1029/2008TC002341.

Sdrolias, M., and Müller, R.D., 2006, Controls on back-arc basin formation: Geochemistry Geophysics Geosystems, v. 7, no. 4, doi: 101029/2005GC001090.

Siks, B.C., and Horton, B.K., 2011, Growth and fragmentation of the Andean foreland basin during eastward advance of fold-thrust deformation, Puna Plateau and Eastern Cordillera, northern Argentina: Tectonics, v. 30, no. 6, TC6017, doi:10.1029/2011TC002944.

Sobel, E.R., Hilley, G.E., and Strecker, M.R., 2003, Formation of internally drained contractional basins by aridity-limited bedrock incision: Journal of Geophysical Research, v. 108, 2344, doi:10.1029/2002JB001883.

Soler, P., and Bonhomme, M.G., 1990, Relation of magmatic activity to plate dynamics in central Peru from Late Cretaceous to present, *in* Kay, S.M., and Rapela, C.W., eds., Plutonism from Antarctica to Alaska: Geological Society of America Special Paper 241, p. 173–192.

Somoza, R., 1998, Updated Nazca (Farallon)–South America relative motions during the last 40 Ma: Implications for mountain building in the central Andean region: Journal of South American Earth Sciences, v. 11, no. 3, p. 211–215, doi:10.1016/S0895-9811(98)00012-1.

Stacey, J.S., and Kramers, J.D., 1975, Approximation of terrestrial lead isotope evolution by a two-stage model: Earth and Planetary Science Letters, v. 26, p. 207–221, doi:10.1016/0012-821X(75)90088-6.

Starck, D., and Vergani, G., 1996, Desarrollo tecto-sedimentario del Cenozoico en el sur de la Provincia de Salta, Argentina, *in* XIII Congreso Geológico Argentino y III Congreso de Exploración de Hidrocarburos: Buenos Aires, Argentina, Actas I, p. 433–452.

Steinmann, G., 1929, Geologie von Peru: Heidelberg, Germany, Karl Winter, 448 p.

Stern, C.R., 1991, Role of subduction erosion in the generation of Andean magmas: Geology, v. 19, p. 78–81, doi:10.1130/0091-7613 (1991)019<0078:ROSEIT>2.3.CO;2.

Strecker, M.R., Alonso, R.N., Bookhagen, B., Carrapa, B., Hilley, G.E., Sobel, E.R., and Trauth, M.H., 2007, Tectonics and climate of the southern central Andes: Annual Review of Earth and Planetary Sciences, v. 35, p. 747–787, doi:10.1146/annurev.earth.35.031306.140158.

Torsvik, T.H., Rousse, S., Labails, C., and Smerhurst, M.A., 2009, A new scheme for the opening of the South Atlantic Ocean and the dissection of Aptian salt basin: Geophysical Journal International, v. 177, no. 3, p. 1315–1333, doi:10.1111/j.1365-246X.2009.04137.x.

Trumbull, R.B., Riller, U., Oncken, O., Scheuber, E., Munier, K., and Hongn, F., 2006, The time-space distribution of Cenozoic volcanism in the south-central Andes: A new data compilation and some tectonic implications, *in* Oncken, O., Chong, G., Franz, G., Giese, P., Götze, H., Ramos, V.A., Strecker, M.R., and Wigger, P., eds., The Andes—Active Subduction Orogeny: Berlin, Springer-Verlag, Frontiers in Earth Sciences, v. 1, p. 29–43.

Uba, C.E., Heubeck, C., and Hulka, C., 2006, Evolution of the late Cenozoic Chaco foreland basin, southern Bolivia: Basin Research, v. 18, p. 145–170, doi:10.1111/j.1365-2117.2006.00291.x.

Vandervoort, D.S., Jordan, T.E., Zeitler, P.K., and Alonso, R.N., 1995, Chronology of internal drainage development and uplift, southern Puna Plateau, Argentine central Andes: Geology, v. 23, p. 145–148, doi:10.1130/0091 -7613(1995)023<0145:COIDDA>2.3.CO;2.

Veizer, J., Ala, D., Azmy, K., Bruckschen, P., Buhl, D., Bruhn, F., Carden, G.A.F., Diener, A., Ebneth, S., Godderis, Y., Jasper, T., Korte, C., Pawellek, F., Podlaha, O.G., and Strauss, H., 1999, Sr-87/Sr-86, $\delta^{13}C$ and $\delta^{18}O$ evolution of Phanerozoic seawater: Chemical Geology, v. 161, p. 59–88, doi:10.1016/S0009-2541(99)00081-9.

Zandt, G., Gilbert, H., Owens, T.J., Ducea, M., and Saleeby, J., 2004, Active foundering of a continental arc root beneath the southern Sierra Nevada in California: Nature, v. 431, p. 41–46, doi:10.1038/nature02847.

Zhou, J., and Lau, K.M., 1998, Does monsoon climate exist over South America?: Journal of Climate, v. 11, p. 1020–1040, doi:10.1175/1520 -0442(1998)011<1020:DAMCEO>2.0.CO;2.

Zhou, R., Shoenbohm, L.M., and Cosca, M., 2013, Recent, slow normal and strike-slip faulting in the Pasto Ventura region of the southern Puna Plateau, NW Argentina: Tectonics, v. 32, p. 19–33, doi:10.1029/2012TC003189.

Geological Society of America Memoirs Online First

The growth of the central Andes, 22°S–26°S

J. Quade, M.P. Dettinger, B. Carrapa, P. DeCelles, K.E. Murray, K.W. Huntington, A. Cartwright, R.R. Canavan, G. Gehrels and M. Clementz

---

Email alerting services	click www.gsapubs.org/cgi/alerts to receive free e-mail alerts when new articles cite this article
Subscribe	click www.gsapubs.org/subscriptions to subscribe to Geological Society of America Memoirs
Permission request	click www.geosociety.org/pubs/copyrt.htm#gsa to contact GSA.

Notes